KeAi

CHINESE ROOTS
GLOBAL IMPACT

Contents lists available at ScienceDirect

Petroleum Science

journal homepage: www.keaipublishing.com/en/journals/petroleum-science



Original Paper

Rheo-optic in situ synchronous study on the gelation behaviour and mechanism of waxy crude oil emulsions



Jian Zhao, Xiao-Feng Li, Hang Dong*, Zhi-Hua Wang

Young and Middle-aged Innovation Team Program of Northeast Petroleum University, Energy-saving and Consumption-reducing Laboratory, Surface Engineering Pilot Test Center of CNPC, Northeast Petroleum University, Daging, Heilongjiang 163318, China

ARTICLE INFO

Article history: Received 14 March 2022 Received in revised form 14 June 2022 Accepted 26 August 2022 Available online 14 September 2022

Edited by Jia-Jia Fei

Keywords:
Waxy crude oil emulsion
Rheo-optic in situ synchronous
measurement
Gelation
Microscopic mechanism
Structural behaviour

ABSTRACT

An improved rheo-optic in situ synchronous measurement system was employed to investigate the gelation behaviour and mechanism of waxy crude oil emulsions. By combining transmitted natural light and reflected polarized light microscopy, a multiangle composite light source was built to achieve the simultaneous observation of wax crystals and emulsified water droplets, as well as their dynamic aggregation process. Main outcomes on the microscopic mechanism were obtained by developed microscopic image processing method. It was found that the microstructure of W/O waxy crude oil emulsion has the evolution of "individual structure-homogeneous aggregate structure-heterogeneous coaggregate structure-floc structure" during the static cooling, which results in the four stages during gelation process. Different from previous studies, the aggregation of emulsified water droplets was found to be more significant and contributes to the formation and development of the wax crystals-emulsified water droplets coaggregate, which plays a decisive role in the further evolution of the gelled microstructure. Time series microscopic images show the dynamic aggregation of emulsified water droplets and wax crystals. Two different aggregation behaviours between wax crystals and water droplets were observed. That wax crystals can not only embed in gaps between adjacent water droplets and enhance the structure, but also surround the outside of the water droplets and continue to grow resulting in the interconnection of different coaggregates to form a larger floc structure. In addition, correlation between viscoelasticity and microstructure evolution of waxy crude oil emulsions of different water contents was discussed. With increasing water contents, the microstructure is changed from wax crystal flocculation structure as the main skeleton and the emulsified water droplets embedded in it, into the aggregation of emulsified water droplets occupying the main position. When the number of wax crystals and water droplets reaches a certain ratio, did wax crystals form coaggregates with emulsified water droplets, and the remaining wax crystals formed an overall flocculation structure, the viscoelasticity of the waxy crude oil emulsion is the highest.

© 2023 The Authors. Publishing services by Elsevier B.V. on behalf of KeAi Communications Co. Ltd. This is an open access article under the CC BY-NC-ND license (http://creativecommons.org/licenses/by-nc-nd/4.0/).

1. Introduction

Oil and gas resources play a pivotal role in the development of the national economy and people's daily lives. In 2020, 65 oil and gas fields were discovered in the world's oceans, with total recoverable reserves of 1.42 billion tons of oil equivalent, accounting for 73.0% of the total new global reserves (Yu et al., 2021). With the significant progress made in offshore oil and gas exploration in

recent years, an increasing number of countries has expressed their interest in deep-water oil production. Crude oil inevitably mixes with water during the exploitation process, and the mixture easily forms an emulsion as it passes through the wellbore, nozzle, and pipeline. Emulsions of waxy crude oil is more easily to gel in low-temperature environments, which poses a threat to the safety of pipeline operation. Therefore, studying the gelation behaviour and mechanism of waxy crude oil emulsions is necessary.

Scholars (Jiang and Li, 2000; Sun and Zhang, 2016; Wen et al., 2016; Piroozian et al., 2021) have long recognized that the apparent viscosity of emulsions is closely related to various factors, such as water and asphaltene contents, shear rate, and temperature.

^{*} Corresponding author. Northeast Petroleum University, Xuefu Street NO.99, Hitech Development Zone, Daqing, Heilongjiang 163318, China. *E-mail address*: dh.123@163.com (H. Dong).

With the increasing focus on rheological research on waxy crude oil emulsions and the needs of practical engineering, scientists and engineers have begun to pay more attention to the structural behaviours of waxy crude oil emulsions, such as yielding, thixotropy, and viscoelasticity (Haj-shafiei et al., 2013; Sun et al., 2014, 2017; Guo et al., 2016, 2021). The most direct factor affecting the rheology of waxy crude oil emulsions is water content, which has been studied in detail by scholars. Some studies have found that the structural strength of waxy crude oil emulsions is inversely proportional to temperature and proportional to water content (Visintin et al., 2008; Huang and Wang, 2013; Zhang et al., 2019). Additionally, some scholars have found that the structural strength of waxy crude oil emulsions is inversely proportional to the water content (Peng et al., 2009; Oh and Deo, 2011). Furthermore, some scholars have proposed that the strongest waxy crude oil emulsion gel structure has the most appropriate water content and the structural strength of the system increases or decreases with the volume fraction of the dispersed phase, depending on the content of solid particles (Paso et al., 2009; Dickinson, 2012). A waxy crude oil emulsion is a multicomponent dispersed phase system. The state of the discrete phase present in the continuous phase has a strong correlation with the rheological properties of the system. Some studies have shown that the oilwater interfacial tension of the emulsion has a considerable impact on the viscoelasticity of the system, and fine emulsions have higher values of the viscosity and storage moduli than coarse emulsions (Pal, 1996; Lee et al., 1997). Some scholars have relieved that the enhanced viscoelasticity of emulsions is caused by bridging or flocculation between droplets or wax crystals in the system (Schramm, 1992: Ma et al., 2019). The increase in the elastic behaviour led to decrease in coalescence mechanism among the emulsions, and thereby producing the stable emulsion (Wong et al., 2015). Several scholars have analysed the mechanism of the behaviour of waxy crude oil emulsion gelation structures based on experimental results and related theories. Emulsions with higher cooling rates have two critical stress structures, and the research show that the first yield point is related to network rupture and the second yield point is related to cluster breaking (Koumakis and Petekidis, 2011; Vargas et al., 2018). The brittle fractures form between wax crystals and flexible fractures are present between droplets and wax crystals was proposed (Guo et al., 2016, 2021). The macroscopic rheological behaviour of waxy crude oil emulsions could be attributed to wax crystal particles, dispersed water droplets, or the interaction between the two (Zhang et al., 2010; Sun et al., 2014, 2017). Therefore, although scholars have a relatively comprehensive understanding of the macroscopic rheological properties of waxy crude oil emulsions, there is still no consensus on the understanding of some rheological behaviours. Regarding the generation mechanism of the complex rheological behaviour of waxy crude oil emulsions, most research relies on relevant theories based on the analysis of experimental

In recent years, with the development of microscopic observation technology and the emphasis on studying waxy crude oil emulsion microstructure, some scholars have used new experimental techniques and methods (Schramm, 1992; Visintin et al., 2008; Blake and Marangoni, 2015; Li et al., 2015; Shi et al., 2018; Liu et al., 2019; Fan et al., 2021) to conduct relevant research on the microstructure of waxy crude oil emulsions. The parameters such as droplet size and particle size distribution through quantitative analysis of microscopic droplets in emulsions under an optical microscope were obtained (Huang and Wang, 2013). The pre-sheared oil samples under the microscope were observed and founding that shearing reduced the wax crystal size and increased the complexity of the wax crystal structure (Blake and Marangoni, 2015). Some scholars (Shi et al., 2018) used focused beam reflectance measurement (FBRM) and particle vision and measurement (PVM) techniques to make

microscopic observations of emulsion droplets and wax crystals. The microscopic images of droplets and wax crystals were obtained by combining polarized light and light transmission techniques and observed wax crystals and droplets by segmenting and splicing the images (Liu et al., 2019; Fan et al., 2021).

Microscopic observation is the primary method used to study the microstructure of waxy crude oil emulsions. However, due to the considerable differences in the optical properties of wax crystals and emulsified water droplets, it is difficult to refine their microscopic features, spatial distribution and aggregate structures. At present, microscopic observation technology such as microscopes are mainly used to make observations. Rheological measurements are made with a rheometer, and the results from the two methods are correlated. However, because researchers use different experimental instruments, differences in the properties and states of the samples in the rheological and microscopic experiments influence the synchronisation of the rheological and microscopic results. If microstructure changes can be observed in situ while rheological measurements are performed, then the accuracy of the rheo-optic correlation analysis will inevitably be improved, and a more accurate conclusions will be obtained from microscopic analyses of mechanisms. In other fields, some scholars have achieved notable research results using in situ synchronous microscopic observation methods. For example, the fluorescent signals of markers in real time were tracked while applying force to bacterial cell walls using an atomic force microscope. Linking macroscopic forces to microscopic dynamics provided a more comprehensive understanding of the effects of mechanical forces on bacteria (Del Valle et al., 2020). The real-time in situ microscopic observations of GM-3 liner material was performed to understand its contact characteristics and wear mechanism at different contact pressures and sliding speeds (Feng et al., 2017). An interfacial stress rheometer was built to measure the rheological properties of suspensions while tracking the particles, studied the uniform evolution of amorphous systems at the particle level under oscillatory shear, and linked this evolution to macroscopic rheology (Teich et al., 2021). A new uniaxial or biaxial uniform confocal rheometer was designed that can image 3D structure of materials using high-speed confocal microscopy and simultaneously monitor stress data on a rotating axis (Lin et al., 2014).

Based on the above analysis of research, there is still no consensus on the understanding of the gelation behaviour of waxy crude oil emulsions, and the analysis of its microscopic mechanism has not been satisfactorily resolved. Concurrently, there have been technical advances and outstanding achievements using in situ microscopy and synchronous experimental measurements in related fields. In this study, a rheo-optic in situ synchronous measurement system was modified by improving the light source of the rheometer, combining transmitted light and reflected light microscopy, polarized light and natural light and building a multiangle composite light source and used for the synchronous observation of wax crystals and emulsified water droplets. Based on the improved experimental system, an in situ synchronous experimental study was conducted on the viscoelastic parameters and microstructure evolution during the cooling and gelation of waxy crude oil emulsions with different water contents. Based on the experimental results, microstructure evolution during the waxy crude oil emulsion gelation processes was divided into four stages. The structural characteristics, aggregation behaviour, and dynamic formation process of the aggregation structure of wax crystals and emulsified water droplets in each stage were analysed in detail. Based on this approach, the waxy crude oil emulsion gelation mechanisms were analysed. The microscopic mechanism of how water content affects gelation behaviour of waxy crude oil emulsions was discussed in detail.

2. Experimental materials and methods

2.1. Experimental materials

Hulunbuir (H) crude oil (hereafter referred to as H crude oil) and purified water were used to prepare waxy crude oil emulsions. To improve the repeatability and accuracy of the experimental results and remove the "historical memory" of H crude oil, H crude oil has been pretreated before the experiment (Yan and Luo, 1987; Guo et al., 2015; Li et al., 2015). H crude oil was first sealed in reagent bottles then were heated to 80 °C in a constant temperature water bath, kept this temperature for 2 h, and then naturally cooled to room temperature and stored for more than 48 h. Referring to most research, it is generally believed that at this pretreated temperature, wax crystals were fully dissolved, resins and asphaltenes were fully activated. Thus, the thermal history effects such as heating, cooling, and repeated heating, as well as the shear history effects experienced by waxy crude oil in the process of production and transportation were removed. After this procedure, a group of oil samples with the same initial state have been obtained, which can improve the repeatability of subsequent experimental results. Experimental errors have also been reduced, so that the comparison and analysis of experimental results was more accurate.

Before preparing waxy crude oil emulsions, it was necessary to clarify the physical and chemical properties of the oil. According to GB/T 2013–2010, the density of H crude oil at 20 °C was 835.6 kg/m³. According to SY/T 0545–2012, using differential scanning calorimetry (DSC), the wax appearance temperature (WAT) of H crude oil was determined to be 47.0 °C, and the wax content was 16.34%. According to SY/T 5119–2016, using the column separation method, the saturated hydrocarbon content of H crude oil was 65.8%, the naphthenic hydrocarbon content was 18%, the resins content was 11.8%, and the asphaltene content was 4.4%. According to ASTM D5853-11, using a crude oil pour point tester, the pour point of H crude oil was determined to be 21 °C. According to ASTM D7169-18, using a gas chromatograph, it was determined that the content of H crude oil below C₃₇ was 68.91%, and the content above was 10.09%.

2.2. Experimental method

2.2.1. Experimental instrument

The emulsion was prepared by mechanical stirring, using an IKA RW20 digital stirrer produced by the IKA Company of Germany, equipped with a four-blade inclined paddle. The rotational speed precision was 0.01 rpm. An SC/AC-S constant temperature water bath from Thermo Fisher Company of the United States, with a temperature control accuracy of 0.01 $^{\circ}$ C, was used to prepare the emulsions. An electric blast thermostat was used to preheat oil samples. The rheometer was an MCR 702 Twin Drive modularization rheometer from Anton Paar, Austria. In addition to the rheological measurement function, it was equipped with a synchronous *in situ* microscopic observation module.

2.2.2. Preparation of W/O waxy crude oil emulsion

The water used to prepare the emulsion in the research was purified water. Before the emulsion was prepared, the fluidity of the pretreated and cooled oil sample must be restored. The oil samples were sealed and placed in the thermostat at 70 °C and kept constant, then transferred to a water bath at 50 °C. In previous study (Dong et al., 2020), it has been found that after cooling the oil sample at 70 °C, the wax crystals formed have more distinct structural characteristics and the reflection effect of light was better. Higher quality microscopic images could be obtained so that the subsequent research on the microstructural properties of waxy

crude oil emulsion was more accurate. In addition, since the emulsion preparation temperature was 50 °C, considering the temperature drop during the oil sample transfer, the heating temperature of the oil sample before the emulsion preparation should be higher than 50 °C. After the sample temperature was uniform and stable, appropriate volumes of H crude oil and purified water were measured in a predetermined ratio and placed in different beakers. The beakers were sealed and placed in a constant temperature water bath, and the emulsion preparation was started after the oil and water reached the predetermined temperature. The mechanical stirring method was selected, and the specific oilwater ratio mixture was continuously stirred for a certain period at a fixed stirring rate to prepare an emulsion. In this study, each emulsion was prepared by one-time addition of water and mixed with a digital stirrer while the stirring speed and time were strictly controlled. Notably, the emulsion preparation temperature should be above the WAT to prevent destruction of the wax crystal structure and influence of the rheological test results. However, the preparation temperature should not be too high because it could weaken the strength of the oil-water interfacial film and cause the stability of the emulsion to deteriorate. The preparation temperature of the emulsion selected in this experiment was 50 °C, the stirring speed was 1000 rpm, the stirring time was 15 min, and emulsions with different oil-water ratios were prepared with the volumetric water content. The emulsion preparation temperature was 50 °C, which was higher than the WAT (47.0 °C). At the preparation temperature, the wax crystals have not been precipitated. Thus, the shear history effect by the mechanical stirring can not affect the subsequent experimental results (Xia and Zhang, 2001: Kane et al., 2003). Therefore, the repeatability and accuracy of rheooptic in situ synchronous experimental results can be further ensured. To prevent the light components from volatilizing due to mechanical stirring, the emulsion preparation temperature should not be too high. Furthermore, according to previous attempts, the structure of the emulsion prepared at 50 °C can keep stable during the entire experiment. The water contents of the final prepared emulsions included 10%, 20%, 30%, 40%, and 50%.

2.2.3. Rheo-optic in situ synchronous measurements

An MCR 702 Twin Drive modularization rheometer from Anton Paar was used for the rheo-optic in situ synchronous measurements experiment. It was equipped with a microscopic observation system combined with a rheological measurement unit to form a rheooptic in situ synchronous measurement system. Changes in internal microstructure of a sample were observed in situ with a microscope while rheological data were measured by applying precise shear to the sample. Video images were captured by a charge-coupled device (CCD) camera and transmitted to a computer terminal. The overall structure of the measurement system is available in the literature (Zhao et al., 2020). Its core components are shown in Fig. 1. A parallel plate measurement system made of transparent quartz glass was used for rheological measurements; it was driven by the upper motor head of the rheometer to apply precise shear to the sample. It synchronously measured the macroscopic rheological data of the sample. The lower plate was also made of transparent quartz glass, but it served as an objective table to hold the sample. When the instrument lowered the upper rotor to a certain height, a thin liquid layer formed between the upper rotor and the lower stage as the measurement object. A polarizing microscope was installed under the stage with a 20x objective lens, a focal length of 30.9 mm, a depth of field of 1.6 µm, and optical compensation to achieve a resolution of 0.7 µm and an observation field size of 440 $\mu m \times 330 \ \mu m$. The microscope was integrated with a 150 W-LED light source that irradiated the sample vertically from the lower part of the lens, entered the microscope after reflection,

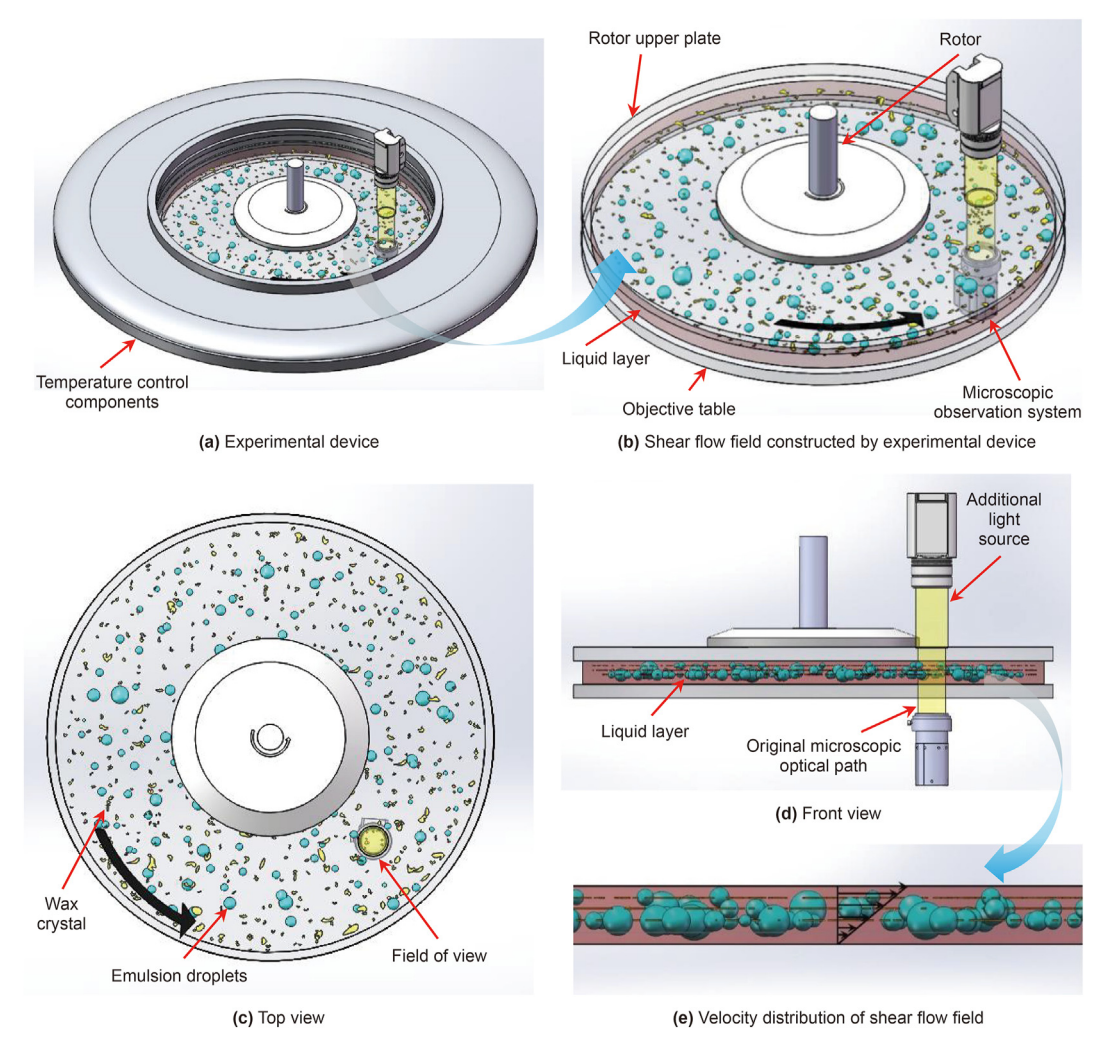


Fig. 1. Schematic diagram of the experimental device.

and took microscopic images of the sample. The lower part of the microscope was also integrated with a CCD camera from Lumenera, and the frame rate was 15.19 frames/s. The CCD camera was connected to the computer through data cables, and the captured images or videos could be transmitted to the computer software for real-time viewing or storage. It was necessary to precisely control the sample temperature and its rate of change during the experiment. The temperature control unit of the instrument consisted of two parts. One part was a Peltier temperature control unit installed around the stage. The temperature control accuracy was 0.01 °C, and the control range was $-20\,^{\circ}\text{C}-200\,^{\circ}\text{C}$. In addition, to ensure a uniform temperature inside the sample, the instrument was equipped with a synchronous temperature control cover, which covered the sample from the upper part of the sample.

When the measurement system was applied to observe waxy crude oil emulsions, due to the different physical and chemical properties and light reflection properties of wax crystals and emulsified water droplets, they could not be photographed at the same time using the light source provided originally with the instrument. Therefore, to achieve simultaneous observations of wax crystals and emulsified water droplets, based on the existing polarized light source, an additional natural light source was added above the sample. The two light sources simultaneously illuminated the sample vertically from different directions. In this way, the mixture of natural and polarized light and the combination of

transmission and reflection microscopy were realized to simultaneously observe wax crystals and emulsified water droplets. Fig. 2 shows the difference in images that were photographed before and after adding the light source. The simultaneous observations of wax crystals and emulsified water droplets was realized by increasing the light source, and the observation quality of wax crystal was greatly improved. Fig. 1 shows a structure diagram of the improved rheo-optic *in situ* synchronous measurements system after the light source was added from different perspectives. A standard Couette flow field formed within the microscopic field of view. The upper plate rotor drove the upper surface of the sample to move at a fixed speed, and the lower plate was in a static state. A linear shear flow field formed inside the sample.

2.2.4. Experimental measurement procedure

The experiment mainly measured the variation of viscoelastic parameters of emulsions with different water contents during the process of cooling at a constant rate in the small amplitude oscillating shear (SAOS) measurement mode, in synchronisation with the entire rheological test process. The dynamic evolution of the microstructure in the emulsion during the rheological test was observed *in situ* with a microscopic observation system, and video images were taken. The specific operating procedures were as follows:

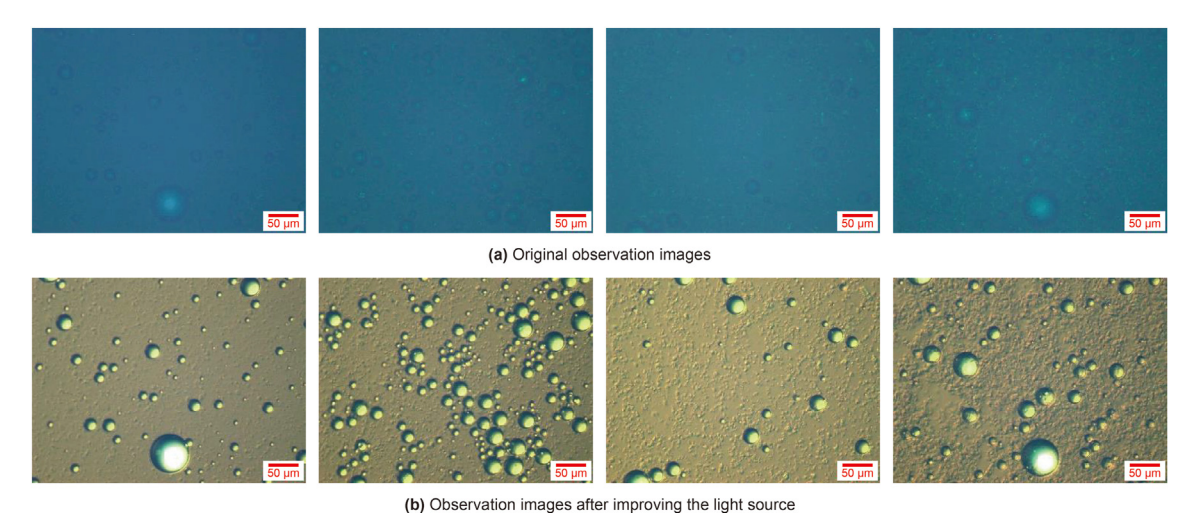


Fig. 2. Comparison of the shooting results before and after the MCR702 rheometer composite light source.

- (1) The preset temperature of the rheometer was the initial cooling temperature of the experiment, 40 °C. An appropriate amount of the synchronously prepared fresh emulsion was quickly transferred to the objective table and allowed to stand at a constant temperature on the stage for 5 min to make the internal temperature of the sample reach a uniform and stable state.
- (2) The experimental instrument was controlled so that the sample temperature decreased to a final cooling temperature of 16 °C at a preset rate of 0.5 °C/min. The rheological measurement unit was controlled to measure the rheological data such as the storage and loss moduli (*G'* and *G''*) of the sample with temperature in the SAOS mode. The strain amplitude for the SAOS mode was selected according to the logarithmic relationship with decreasing temperature, from 1% to 0.01%, and the oscillating frequency was constant at 10 rad/s
- (3) At the same time as the above rheological measurements, the microstructure changes inside the sample were observed synchronously, and video images were captured and stored.

The water contents of the emulsions involved in the experiment were 10%, 20%, 30%, 40%, and 50%. The initial cooling temperature of the experiment was 40 °C, the cooling rate was 0.5 °C/min, and the final cooling temperature was 16 °C. Each experiment was repeated at least twice to ensure the repeatability and measurement accuracy of the results.

The purpose of this research is to reveal the evolution of the microstructure during the gelation of emulsions, especially to capture the process of precipitation, aggregation, growth of wax crystals and their flocculation with water droplets. Therefore, the experimental initial cooling temperature cannot be too low that many wax crystals have been precipitated. In addition, the prepared 50 °C emulsion needs to be transferred to the rheometer stage at room temperature (about 20 °C), which causes the temperature drop of the sample. If the temperature of the stage is too high, the sample that has been cooled during the transfer process will be heated repeatedly, thereby introducing additional thermal history effects, and affecting the accuracy and repeatability of the subsequent experiments. After many attempts, 40 °C was applied as the initial temperature of the emulsion rheo-optic in situ synchronous study.

2.2.5. Comparison and verification of microscopic observations

The in-situ observation of waxy crude oil emulsion microstructures was the focus of this paper. In other studies, most scholars used the method of first sampling the waxy crude oil emulsion to make specimens on glass slides and then observing the microstructure offline with a transmission polarizing microscope (Visintin et al., 2008; Liu et al., 2019; Fan et al., 2021). In recent years, some scholars have used PVM technology to observe the microstructure of waxy crude oil emulsions in situ. To verify the effect of the microscopic observation system used in this paper and compare it with current technology, the observations and results obtained with different experimental instruments are listed in Fig. 3. The observations that were made using a transmission polarizing microscope were obtained by preparing a film in the experimental sample for observation. The selected instrument was a polarizing microscope (Nikon ECLIPSE LV100NPOL), the objective observation lens was 20 times, and the observation accuracy was 0.001 µm. The observation made with PVM were obtained by directly plugging the instrument into the experimental sample. The chosen instrument was from Mettler. The observations made with the MCR702 were obtained by adding the sample to the objective table of the experimental equipment for direct observation using the rheo-optic in situ synchronous measurement system of the MCR 702 rheometer.

Fig. 3 shows observations made with different experimental techniques to observe water droplets in the emulsions; the observed water droplets were similar in shape. However, their spatial distributions and the observation effects were quite different. In the observations made with the transmission polarizing microscope, the emulsified water droplets were more discrete. Because the specimen was a film, many water droplets were squashed, and their shapes changed. In contrast, in the image water droplets distributed in different liquid layers, the bottom water droplets could not be photographed clearly. Due to poor light transmittance of crude oil, the observation field of PVM was dark, and the observations were not clear enough. Nevertheless, PVM distinguished the presence of many closely packed droplets in the image. Since the samples were observed in situ, no water droplets were damaged, and the observed water droplets were relatively complete in structure and had a certain three-dimensional shape. In the observations made with the MCR 702 rheometer, the structure of the emulsified water droplets was relatively complete, and

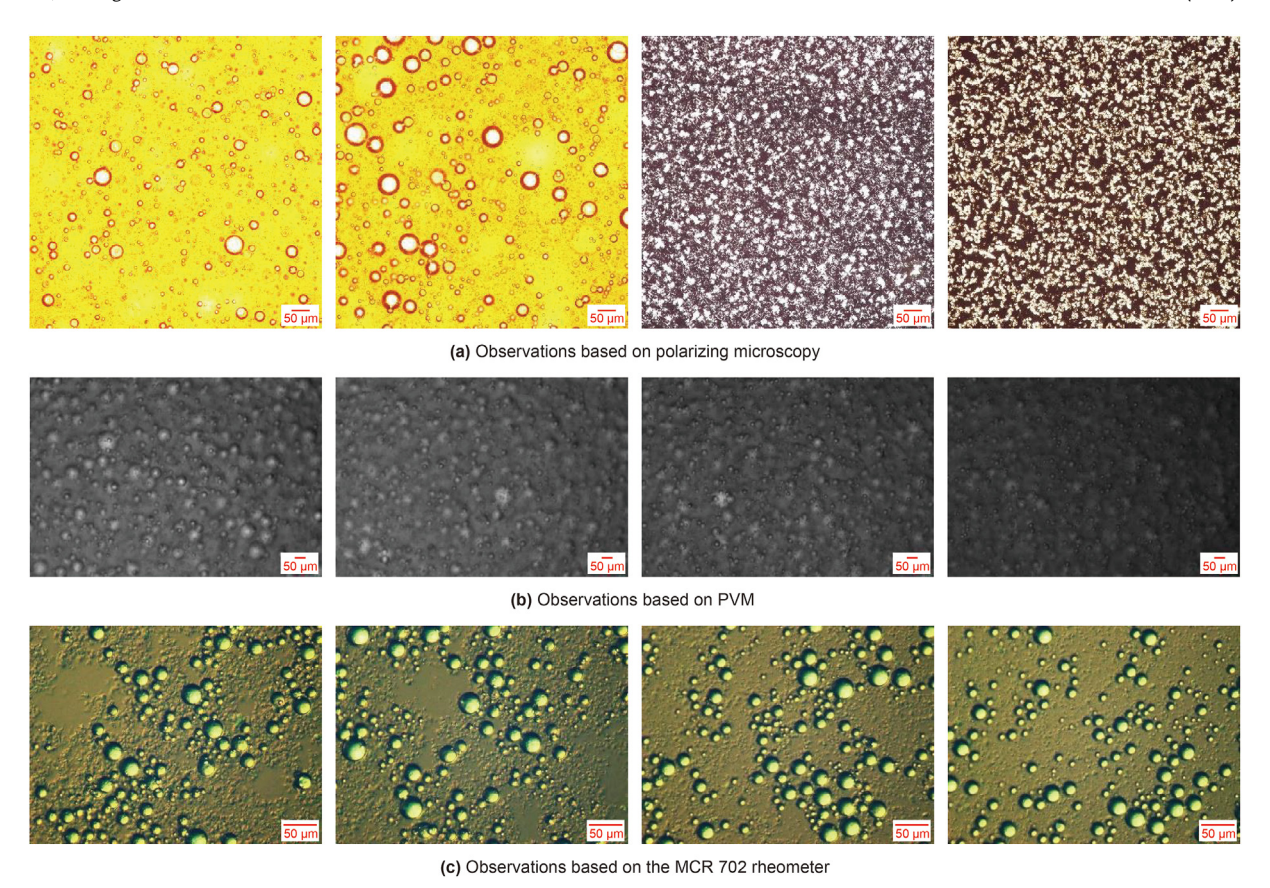


Fig. 3. Comparison of observation results of different experimental instruments.

none of them were crushed. However, in this experimental technique, when the sample was placed on the objective table, it was also necessary to lower the height of the upper plate rotor to exert a certain pressure on the sample to form a thinner liquid layer. However, because the instrument controlled the rate of descent of the rotor, it changed the thickness of the sample at a very slow rate. Since there was no constraint around the sample, the sample had sufficient space and time to spread to the surroundings, thus preventing damage to its internal structure and maintaining its original appearance; the three-dimensional appearance of the emulsified water droplets was similar to that in the PVM results. However, the field of view was brighter, and the observations were more apparent, which was related to the additional light source.

In addition, the transmission polarizing microscope was used to clearly observe wax crystals by changing the polarization angle, and the quality of the images was high. The observation results were clearer for the wax crystals than the water droplets. Unfortunately, the microscopic morphology of the emulsified water droplets could not be obtained simultaneously with the wax crystal images, so the interaction between the two microscopic units and the relative relationship of their spatial structure could not be determined. Since PVM does not have a matching polarizing system, it was almost difficult to distinguish the presence of wax crystals in the image. In contrast, the simultaneous observations obtained with the MCR 702 rheometer, due to the additional light source, the combination of natural light and polarized light sources and the compounding of transmission and reflection light sources, made it possible to identify the presence of wax crystals and emulsified water droplets. In addition, by driving the rotor with a fixed shear strength, the dynamic changes in the sample's internal structure were observed synchronously, and the macroscopic rheological

data were measured simultaneously. Judging from the observations of wax crystals alone, the results obtained by using the MCR 702 rheometer were also relatively straightforward. The morphological structure of wax crystals was basically consistent with the results obtained with the transmission polarizing microscope. Therefore, the above results showed that the observations made with the experimental technique used in this paper were effective and had important advantages.

2.2.6. Repetitive examination and analysis

To improve the repeatability and accuracy of the experimental results, the same pretreat procedure was performed on all oil samples before the formal experiment to remove thermal history and shear history effect. In addition, at least two repeated experiments were performed on each condition to ensure the result reliability, and the relative deviation was shown with error bars in the experimental results. For rheological measurements results, at temperature near the initial cooling temperature, the viscoelasticity data showed certain fluctuation, which was related to the low viscoelasticity value due to the little wax crystals precipitated. This was also mentioned in related research. In this temperature range, no gelling structure formed in the system, so it was not the temperature range that focuses on. As the temperature continued to decrease, the number of wax crystals precipitated increased, the structural performance was enhanced, and the relative deviation of the rheological results was also significantly reduced, and finally stabilized within 10%. The variation trend of the measurement results was unambiguous, and the measurement accuracy could be ensured. Further analysis of the error cause, it should be related to the randomness of wax precipitation and growth. For microscopic images obtained synchronously, to reduce the influence on

quantitative identification caused by different visual fields, at each observation temperature, the microscope was moved to take at least four images of different visual fields. Then, the statistical average of the observation results of different microscopic images was used as the final quantitative identification result, and the corresponding error bars were also given in the subsequent results. The relative deviation of statistical microscopic results found that the maximum was 10.51%, the minimum was 1.37%, and the average was 7.13%. It was found that the measurement accuracy was high, and the overall trend was unambiguous. The results of different observations should be related to the wax crystal precipitation and growth randomness, as well as a small difference in the properties of oil samples.

3. Method for the analysis of experimental results

3.1. Quantitative identification of microscopic images

In the microscopic images taken in this study, although the structural characteristics of wax crystals and emulsified water droplets were directly observed, due to their different optical properties, especially the ability to reflect light, the grey span of emulsified water droplets was larger, while the grey span of wax crystals was smaller and within the grey span of emulsified water droplets. The traditional direct threshold segmentation algorithm cannot realize the accurate quantitative identification of emulsified water droplets and wax crystals at the same time, which will bring about non-negligible identification errors. To address this situation, this study combined several core algorithms, such as "image multilevel optimization processing", "object classification" and "threshold segmentation", took the independent hierarchical threshold segmentation of emulsified water droplets and wax crystals as the basic idea, and constructed a set of eight operating procedures, including "first-level clarity processing of the image", "intelligent classification of objects by the random forest algorithm", "removal of far-focus layer water droplets ", "removal of water droplets from the image", "secondary clarity processing of the image", "image threshold segmentation", "layer comp" and "quantitative recognition of the image". A new method suitable for the accurate identification of microscopic units, such as wax crystals and emulsified water droplets, in microscopic images was developed. The specific implementation process was as follows:

- (1) Original image extraction. According to the needs of the research, video processing software such as Adobe Premiere was used to select the key frames in the video taken in the experiment to obtain original microscopic images, as shown in Fig. 4(a).
- (2) First-level clarity processing of the image. The application of Adobe Photoshop software to optimize and adjust the brightness and contrast of the original images made the emulsified water droplets detail information in the image richer and the overall clarity greatly improved; the results of Fig. 4(b) were obtained. The following algorithm achieved this:

$$g(i,j) = \alpha f(i,j) + \beta$$

where, α is the contrast coefficient, which is less than 1 the pixel is darker and greater than 1 the pixel is brighter, and β is the brightness gain variate.

(3) Intelligent classification of objects by the random forest algorithm. Based on the significant difference in greyscale and morphology of emulsified water droplets and wax crystals,

the emulsified water droplets had a higher grev scan in the reflection, a lower grey scan in the shadow, and a prominent roundness. The grey of wax crystal was in the middle range of the grey of the emulsified water droplets and had a complex morphology and a higher irregularity. The random forest intelligent classification algorithm was applied to classify the water droplets in the image with pixel grey such as adjacent pixels, entropy, maximum value, minimum value, and median as the judgment criteria. Then, the identified water droplets were given a specific grey, and the other parts were given a grey that was different from the water droplets. The random forest is a combinatorial classifier algorithm composed of multiple decision tree weak supervision models, which has good classification performance and antinoise ability (Breiman, 2001; Arganda-Carreras et al., 2017). The random forest classification model G(x) was:

$$G(x) = \underset{Y}{\operatorname{argmax}} \sum_{i=1}^{m} I(g_i(x, L_i) = C)$$

where, I(x) is a prescriptive function, C is a classification label, and $\{L_i\}$ is a random vector of independent codistribution.

The random forest algorithm was applied to intelligently classify the objects of the images, and the results were supervised and reclassified several times. The classification results were gradually optimized until the classification error was maintained in a small range. The classified results are shown in Fig. 4(c). As seen from the figure, after classification, the emulsified water droplets were screened individually and given the same colour. At the same time, the remaining objects in the image were uniformly grouped into one category and marked with another colour.

(4) Removal of far-focus layer water droplets and threshold segmentation. "Fourier transform-Butterworth high-pass filter-Fourier inverse transform" were used to screen and remove the emulsified water droplets in the far-focus layer. Butterworth high-pass filter could filter out the lowfrequency spectrum and retain the high-frequency spectrum. The low-frequency spectrum of the image was the blurred part of the image, which corresponds to the emulsified water droplets far away from the focusing layer. The high-frequency spectrum was the sharper edge part of the image, which corresponds to the emulsified water droplets on the focusing layer. After the above series of procedures, the microscopic image (Fig. 4(c)) only has two grey values with significant differences, t_1 and t_2 . Threshold segmentation was performed on them. The selection of the threshold was based on the following:

$$t' = \frac{1}{2}(t_1 + t_2)$$

In this research, t_1 and t_2 were 76 and 189, respectively, which were the greyscale corresponding to red and green in Fig. 4(c). After threshold segmentation (Fig. 4(d)), the quantitative analysis of the image was carried out using FIJI software, which could obtain microscopic quantitative data of emulsified water droplets (or emulsified water droplet aggregates).

(5) Removal of water droplets from the image. Based on the emulsified water droplet threshold image segmented in the previous step to determine its location and morphological characteristics, Adobe Photoshop software was applied to overlap the emulsified water droplet threshold image and the original microscopic image to achieve water droplet

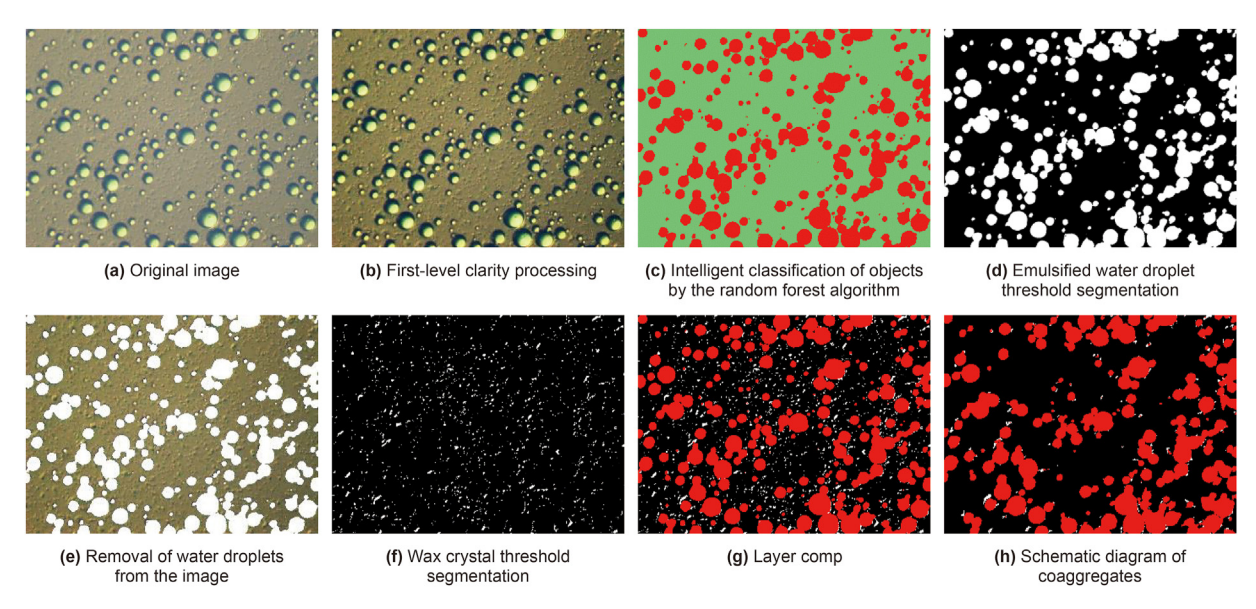


Fig. 4. Microscopic image processing and quantitative identification process.

removal from the image. Emulsified water droplets were removed from the image, and only the liquid hydrocarbons and wax crystals were retained. The results are shown in Fig. 4(e).

(6) Processing of microscopic images for secondary sharpness and segmentation at thresholds. The microscopic image without emulsified water droplets was secondary sharpening, noise reduction, and high pass to improve the quality of the image. Because the emulsified water droplets were removed, the wax crystal threshold image after segmentation had complete structural information. Then, combined with the difference in light intensity in different areas of the image, block threshold segmentation was performed. Here, the threshold segmentation of wax crystal images was based on the current method of our research group (Li et al., 2021; Zhao et al., 2021). Based on the grey value of the image, the maximum entropy threshold segmentation algorithm was used to perform threshold segmentation on the microscopic image blocks. Which has the advantages of wide coverage, retained more image information, better attention to the edge and weak object information, and less neglect and misunderstanding of wax crystal structure. In this algorithm, the optimal threshold value of image segmentation was determined by maximizing the sum of the entropy of the object and background. The selection of the threshold was based on the following:

probability of pixels whose threshold value was more than t. Then, the threshold images after segmentation can be stitched together to obtain the threshold image of wax crystals (Fig. 4(f)). FIJI software was used to quantitatively analyse the microscopic image, which could obtain the quantitative data of wax crystal.

- (7) Layer comp. Adobe Photoshop software was applied to the layer composite operation. The wax crystal threshold image was superimposed on the emulsified water droplet threshold image and distinguished by different colours. Finally, the total image of the dispersion phase threshold of the W/O waxy crude oil emulsion system was obtained. The results are shown in Fig. 4(g).
- (8) Quantitative recognition of the image. For the total threshold image of the dispersed phase obtained in the previous step, programs were written based on stereoscopic methods and computer graphics recognition algorithms and used to finely capture the boundary contours of microscopic units such as wax crystals and emulsified water droplets in the threshold image, quantitatively identify their characteristic geometric parameters, and obtain characteristic morphological data, including microscopic unit geometry, marginal distance, and the aggregation morphology and information about the spatial structure relationship of wax crystals and emulsified water droplets. Fig. 4(h) shows an image of the coaggregate morphological characteristics formed after the aggregation of wax crystals and emulsified water droplets.

$$t^* = \operatorname{argmax}(-\sum_{i=0}^t (p_i/P_t) * \log(p_i/P_t) - \sum_{i=t+1}^{L-1} (p_i/P_{255-t}) * \log(p_i/P_{255-t}))$$

where t^* was the optimal threshold, p_i was the probability of each pixel in the image, P_t was the sum of the probability of pixels whose threshold value was less than t, P_{255-t} was the sum of the

3.2. Extraction of characteristic parameters

For each image after threshold segmentation, Fiji software was used to further obtain morphology data for each microscopic unit.

This study mainly focused on the evolution of the waxy crude oil emulsion gel structure. Therefore, we focused on extracting the area fraction of wax crystals and emulsified water droplets, minimum marginal distance between wax crystals and emulsified water droplets, area fraction of coaggregates formed after wax crystals and emulsified water droplets aggregated, minimum marginal distance of coaggregates and other parameters. The gelation process of waxy crude oil emulsions is characterized by the variation of these parameters with temperature.

3.2.1. Microscopic unit area fraction

Based on the threshold image, the area fraction of each microscopic unit in the W/O waxy crude oil emulsion was obtained. The specific calculation method was as follows:

$$\varphi = \frac{S_i}{S} \times 100\%$$

where, S_i is the area of type i microscopic units and S is the total microscopic viewing area.

This parameter reflects the proportion of each microscopic unit in the waxy crude oil emulsion and is of great significance for understanding the internal structural changes in the system.

3.2.2. Minimum marginal distance

The minimum marginal distance (referred to as marginal distance) represents the minimum distance on the contour line of adjacent microscopic units in the image, as shown in Fig. 5. It can represent the distance between the same or different microscopic units in space, thus reflecting the degree of the compactness of the distribution of units and indirectly reflecting the strength of the interactions of microscopic units. The smaller the marginal distance was, the closer the microscopic units, the narrower the spatial distribution, the easier for the units to come in contact and gather, and the stronger the interaction. To obtain the marginal distance, it was necessary to use a specific search algorithm to find the element closest to the target element by traversing the search and then calculating the distance between the two units according to the coordinates of each point on the two contour lines. The shortest distance was the marginal distance. After the marginal distance of each microscopic unit was obtained, the average marginal distance of all microscopic units was calculated by the statistical average method to represent the spatial distribution characteristics of this microscopic unit.

4. Results and discussion

4.1. Microscopic units within the emulsion

Analysis of the microscopic images at different temperatures and water contents shows that with decreasing temperature, six types of microscopic units formed in the emulsions from wax crystals, emulsified water droplets, liquid hydrocarbons, and their

aggregates, namely, individual wax crystals, individual water droplets, liquid hydrocarbons, wax crystal aggregates, water droplet aggregates, and wax crystal-emulsified water droplet coaggregates.

- (1) Individual water droplets: These units were regular and spherical, single in structure, and strong in light reflection. Their diameter and quantity were related to the preparation conditions of the emulsion.
- (2) Individual wax crystals: Wax crystals precipitated from crude oil as the temperature decreased. The lower the temperature was, the more wax crystals precipitated and the larger their size. The shapes of the wax crystals were very irregular. The difference between wax crystals was significant. The wax crystals easily aggregated, and their light reflection ability was weak.
- (3) Liquid hydrocarbons: They belonged to the continuous phase in the system, that is, a relatively flat and smooth area, as seen in Fig. 6. As the temperature decreased, they were encapsulated by an aggregated structure formed by wax crystals or emulsified water droplets.
- (4) Wax crystal aggregates: As the number of precipitated wax crystals increased, the wax crystal distance decreased, and the wax crystals attracted each other to form an aggregated structure. When wax crystals moved under the influence of thermal convection, they also formed wax crystal aggregates in contact with each other. As the temperature decreased, the number of wax crystal aggregates increased significantly, the coverage gradually grew, and the morphology became more irregular.
- (5) Water droplet aggregates: Emulsified water droplets aggregated under the action of van der Waals forces, especially when the number of water droplets was large and their sizes were small, and the aggregation behaviour was more significant. In addition, when subjected to disturbances such as thermal convection, the emulsified water droplets contacted each other due to movement and formed water droplet aggregates.
- (6) Wax crystal-emulsified water droplet coaggregates: In addition to forming aggregates between similar microscopic units, wax crystals and emulsified water droplets formed coaggregates with different types of units. van der Waals forces were the main reason for the coaggregate structure. In addition, wax crystals and emulsified water droplets moved under the influence of thermal convection in the system, and then contact aggregation occurred. The wax crystal-emulsified water droplet coaggregate structure in Fig. 6 is notable, and it has complex three-dimensional structure. In such aggregates, the water droplets tended to be at the core, and wax crystals grew around the outside of the droplets or were embedded in the gaps between adjacent droplets. The lower the temperature was, the more significant the



Fig. 5. Schematic diagram of marginal distance.

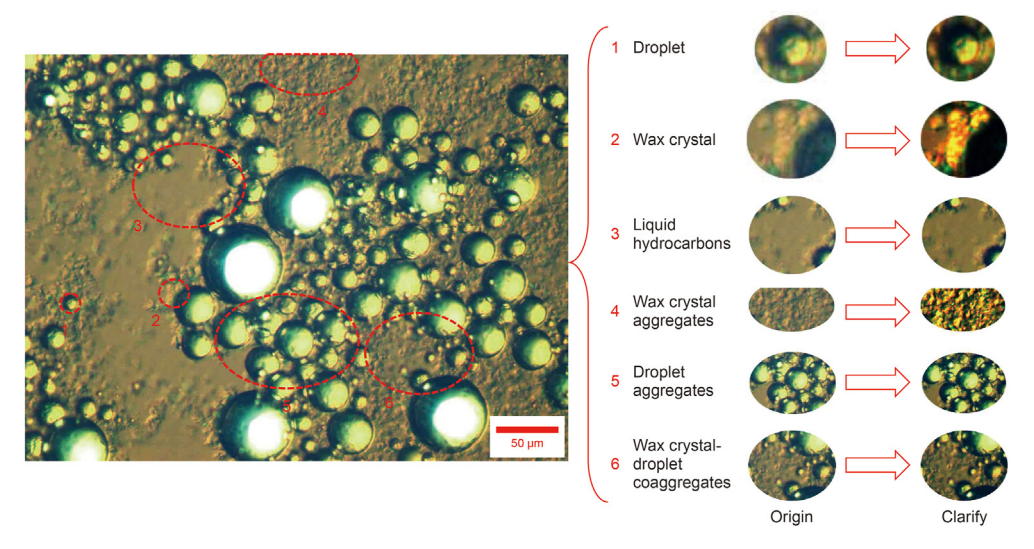


Fig. 6. Microscopic units present in waxy crude oil emulsions.

aggregate structure. It eventually developed into an overall flocculation structure under the continuous precipitation and growth of wax crystals, which had an important impact on the gelation process of the W/O waxy crude oil emulsion.

- 4.2. Microstructure evolution and viscoelastic parameter changes during gelation of waxy crude oil emulsions
- 4.2.1. Results of rheo-optic in situ synchronous experiments

 The changes in the values of viscoelastic parameters and

synchronous microstructure during the cooling and gelation of W/O waxy crude oil emulsions were obtained using the methods of the above experiment. Taking the results of 20% water content as an example, the details were as shown in Fig. 7.

When the temperature was 40 °C, the synchronized microscopic images showed that the number of precipitation wax crystals was minimal, and the viscoelastic values (G', G'') of the system were both low. The growth was slow with the decrease in temperature. The structural behaviour of emulsions was mainly affected by the emulsified water droplets. To ensure the quality of microscopic observation, the thickness of the liquid layer was small, so the

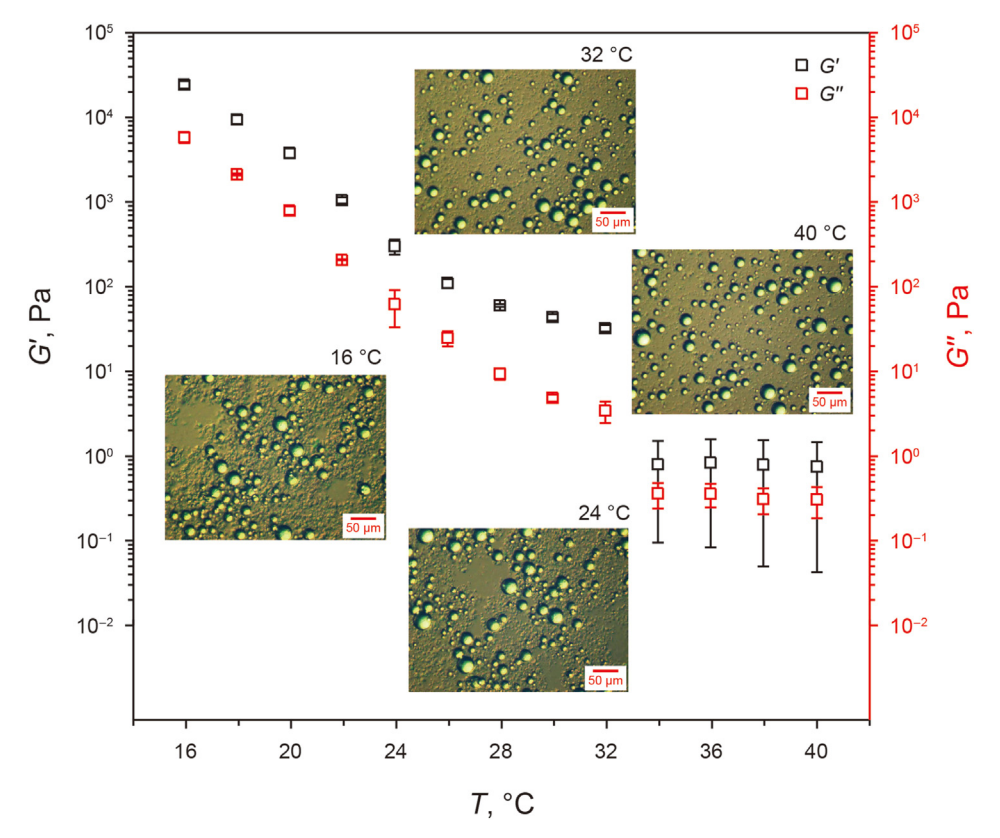


Fig. 7. Rheo-optic in situ synchronous measurement results for a 20% water content emulsion.

influence of emulsified water droplets on the viscoelasticity of the system was enhanced, resulting in a significant error in the rheological data measured in this temperature range. The initial value of G' was higher than that of G'', which was different from the conventional observation results. However, as the temperature gradually decreased to 32 °C, there was a significant increase in the number of wax crystals precipitated in the system, resulting in a significant increase in the measured viscoelasticity data with the decrease in temperature, which could increase by two orders of magnitude. The influence of emulsified water droplets on the structural behaviour of the system was weakened by the precipitation of many wax crystals, which significantly improved the repeatability and accuracy of the measured viscoelasticity data. When the temperature dropped to 24 °C, wax crystals and emulsified water droplets formed coaggregates in the microscopic image. The structure became increasingly complex with decreasing temperature. The coverage increased, causing a significant increase in the growth rate of viscoelasticity data measured with decreasing temperature. There was a significant correlation between the changes in the microstructure of the system and the changes in the macroscopic viscoelasticity data during the cooling and gelation of waxy crude oil emulsions. Therefore, the following discussion focuses on the in-depth analysis of the microstructure evolution of the system to obtain knowledge of the gelation behaviour of waxy crude oil emulsions.

4.2.2. Microstructure evolution during gelation of waxy crude oil emulsion

To prevent random effects, Fig. 8 shows the changes in the microstructure of the emulsion taken from different fields of view as the temperature decreased. Fig. 8 shows that with decreasing temperature, the microstructure of the waxy crude oil emulsion system changed significantly, and there was an evolutionary process of "individual structure-homogeneous aggregate structureheterogeneous coaggregate structure-floc structure", constituting the microscopic performance of its gelation process. The specific trend was as follows: with decreasing temperature, the number of precipitated wax crystals increased significantly, the aggregation behaviour was enhanced, and the aggregation structure became increasingly complex. The aggregation behaviour of emulsified water droplets was significantly enhanced with decreasing temperature. Wax crystals aggregated to the water droplets to form complex coaggregate structures. Affected by the continuous precipitation and growth of wax crystals, the coaggregate structure continued to grow as the temperature decreased and eventually evolved into a floc structure with more extensive coverage and more complex three-dimensional structural properties, which made the strength of the emulsion gel structure continue to increase. To quantitatively illustrate the evolution of the microstructure of waxy crude oil emulsions with decreasing temperature, the analysis method mentioned above was used to extract the area fraction and minimum marginal distance of wax crystals, emulsified water droplets, and their coaggregates with temperature. The details are shown in Fig. 9.

In the early stage of cooling (above 36 °C), the emulsified water droplets in the field of view were very dispersed, and most of them were evenly distributed in the form of individual droplets. The number of wax crystals was small, and most of them were uniformly dispersed in the form of individual particle in the field of view. As the temperature decreased, the aggregation tendency of emulsified water droplets began to increase. It became increasingly significant, resulting in the gradual formation of many water droplet aggregates in the field of view. The number of precipitated wax crystals in the field of view also increased significantly, and the wax crystals were prone to aggregation and tended to aggregate to

water droplets to form coaggregates. The lower the temperature was, the more pronounced this aggregation tendency, and the more complex the formed aggregate structure. With a further decrease in temperature, the wax crystal-emulsified water droplet coaggregate structure became more complex, and the internal microscopic units became increasingly closer. They piled up with each other to show the three-dimensional structural characteristics. In the coaggregates, the water droplets were at the core positions, and some wax crystals surrounded the exteriors of the coaggregates, continued to grow and adsorbed the surrounding wax crystals, thus expanding the coverage of the coaggregates, and finally promoted adjacent coaggregates to come in contact and connect to form a more stable and larger floc structure. Some of the wax crystals filled and stacked in the voids inside the coaggregates to improve the stability and structural strength of the coaggregate structure.

According to Figs. 8 and 9, four stages occurred during the cooling and gelation processes of the W/O waxy crude oil emulsions:

Stage I: Temperature 40 °C-36 °C. As shown in Fig. 8, the emulsified water droplets in the field of view were very dispersed, and most of them were evenly distributed in the form of individual. The number of wax crystals was small, and most of them were uniformly dispersed in the field of view in the form of individual, but there was also a small number of wax crystal aggregates. There were no interactions between most of the wax crystals and emulsified water droplets, and they were relatively independent of each other. However, some wax crystals were close to emulsified water droplets, and they formed a small number of coaggregates with small sizes and a small number of microscopic units. From the quantitative data, at this stage, the area fraction of wax crystals was maintained between 2.05% and 2.44% and increased slightly with decreasing temperature. The average marginal distance of the wax crystals decreased with temperature reduction from 7.33 μm to $6.61 \mu m$. This trend was related to the increase in the number of wax crystals precipitated with decreasing temperature. The area fraction of emulsified water droplets was maintained between 30.98% and 32.45%, and it also showed a slow downwards trend with the reduction in temperature. The average marginal distance was basically stable at approximately 9.92 μm. The decrease in the emulsified water droplet area fraction was related to the increase in the number of wax crystals precipitated with the decline in temperature, and some wax crystals were close to emulsified water droplets to form coaggregates. The area fraction of wax crystalemulsified water droplet coaggregates was between 13.82% and 18.35%, and it increased with decreasing temperature. The increase in its area fraction may be related to image processing. Some wax crystals and water droplets that were close to each other were considered coaggregates, but their connections were not tight. In addition, a small number of wax crystals and emulsified water droplets aggregated at this stage, but coaggregate sizes were small, and most of them formed when a single water droplet was wrapped by wax crystals. Fig. 10 shows the microscopic morphology of the wax crystal-emulsified water droplet coaggregates taken at initial cooling temperature of 40 °C and the subsequent brief cooling process.

Fig. 10 shows that at the initial cooling temperature of 40 °C, although a small number of wax crystals adhered to the surface of the water droplets, they did not entirely cover, and the distribution was not uniform. In addition, it can be found from Fig. 10(a) that wax crystals present not only around the water droplets but also in other positions within the visual field. The precipitation of wax crystals at this temperature were uniformly and randomly distributed. Although the initial crystallization course was not shown in Fig. 10, the outcomes followed by the initial crystallization during 50 °C to 40 °C can still be found in Fig. 10(a). Furthermore,

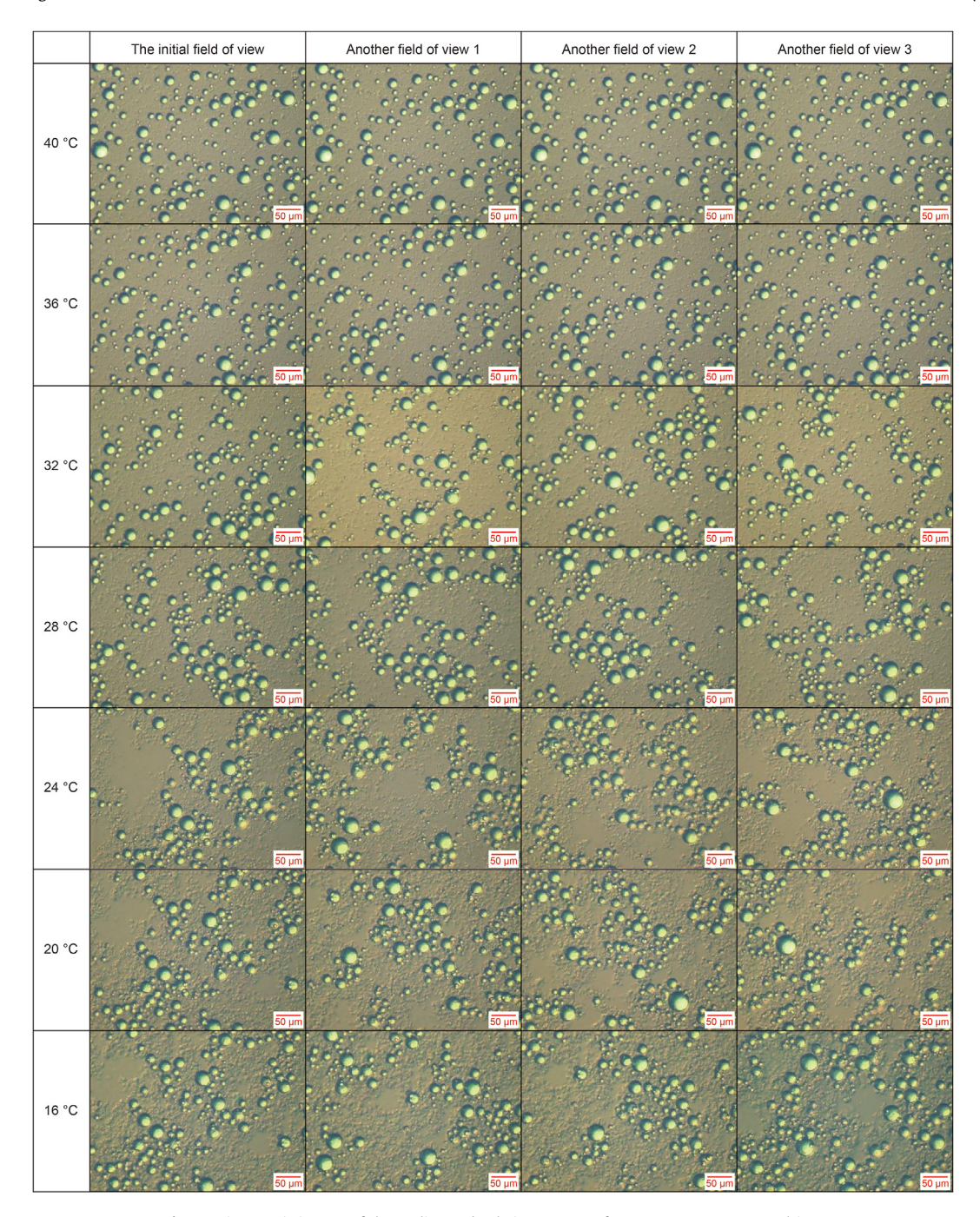


Fig. 8. Microscopic images of the cooling and gelation process of a 20% water content emulsion.

with the temperature decreasing from 40 °C to 36 °C, the number and size of wax crystals adhering to the surface of the water droplets increased slightly. But in general, the concentrated precipitation of wax crystals at the oil-water interface was still insignificant. The number of water droplets covered by wax crystals was still small. The wax crystals were not uniform distributed on the surface of the water droplets. Most of the water droplets and wax crystals were still in a random distribution. Therefore, following the experiment results, the wax crystals adhering to the surfaces of the water droplets may not closely related to the concentrated precipitation of the wax crystals on the surfaces of the water droplets. This is inconsistent with the conclusions of other scholars. We believed that this was due to the different experimental materials,

especially different surfactants from different produced crude oil may contributes the major impact. Based on our experimental results, the movement of the wax crystals driven by thermal convection caused by cooling was the main reason for the wax crystals adhering to the surfaces of the water droplets. Because the wax crystals were smaller than water droplets, and the movement range and strength of wax crystals were much more extensive than those of water droplets. Thus, the moving wax crystals were easily hindered by water droplets and adhered to their surfaces to form coaggregates. This implies that the microscale movement of wax crystals and water droplets should be drawn more attention due to the nonnegligible contribution to the formation of coaggregates.

Stage II: Temperature 36 °C–28 °C. As shown in Fig. 8, the most

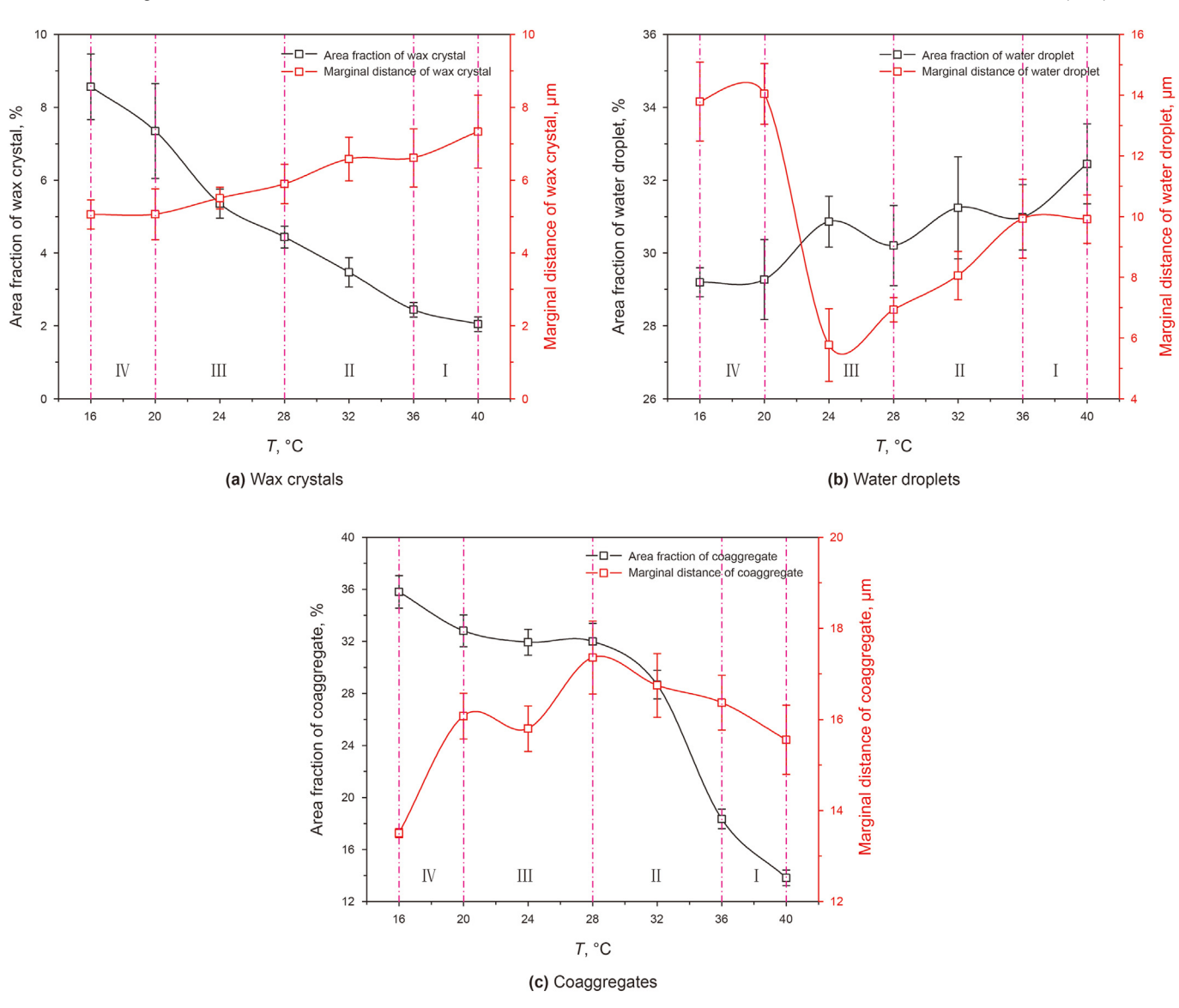


Fig. 9. Microscopic unit area fraction and marginal distance vs. temperature.

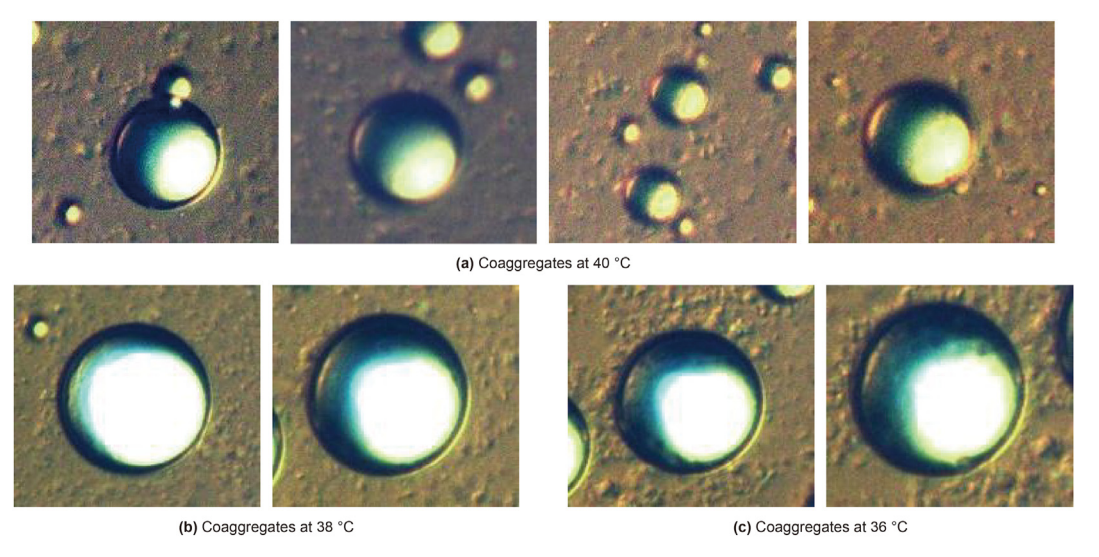


Fig. 10. Micromorphology of wax crystal-emulsified water droplet coaggregates at stage I.

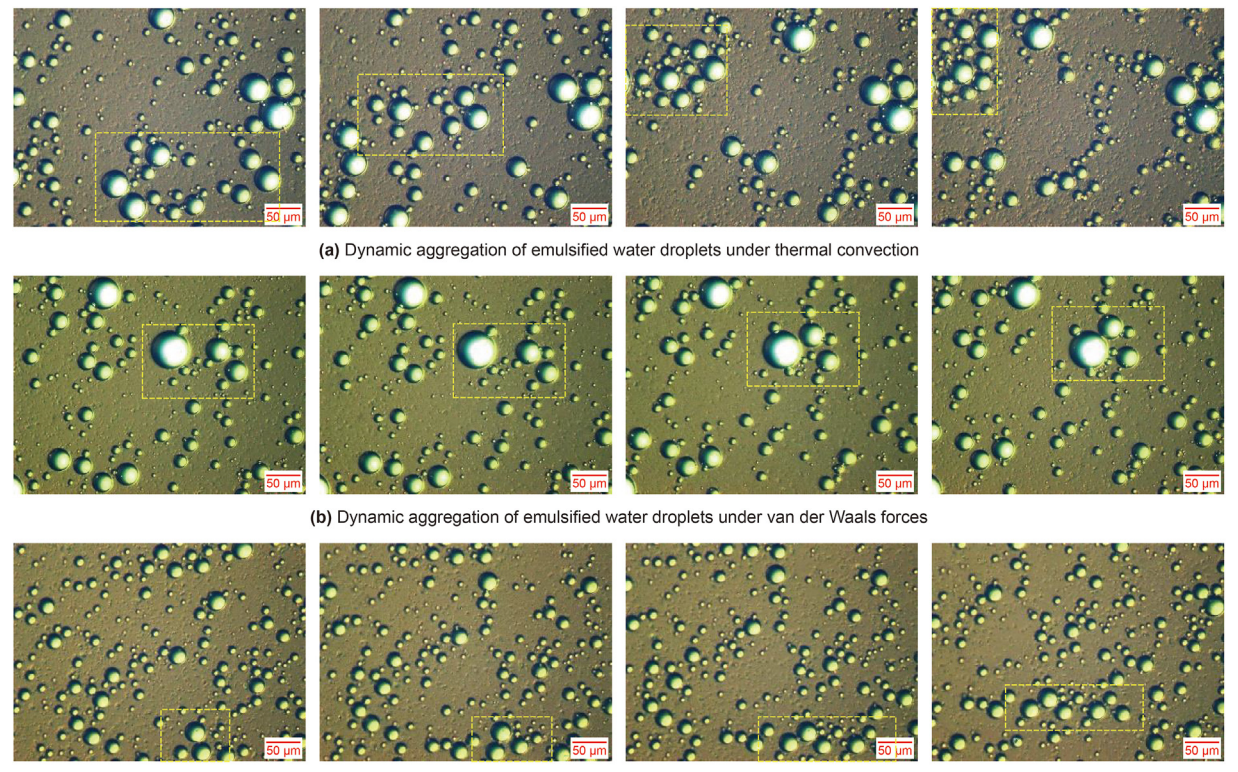
significant phenomenon was that the tendency of emulsified water droplets to aggregate was greatly enhanced, and water droplet aggregates gradually replaced the individual water droplets in the field of view. The number of precipitated wax crystals in the field of view also increased significantly, and the wax crystals were prone to aggregation and tended to aggregate with water droplets to form coaggregates. The lower the temperature was, the more pronounced this aggregation tendency, and the more complex the aggregate structure.

The quantitative data in Fig. 9 show that in this stage, the area fraction occupied by wax crystals increased rapidly, from 2.44% to 4.44%, and the average marginal distance of wax crystals decreased from 6.61 μm to 5.89 μm . The area fraction of emulsified water droplets decreased slightly from 31.23% to 30.20%, while the average marginal distance of water droplets decreased significantly from 9.93 µm to 6.93 µm. The changes in these two parameters indicated that the emulsified water droplets underwent a significant aggregation phenomenon, and some of the water droplets may have come into contact and overlapped, resulting in a decrease in their area fraction. In addition, the area fraction of the wax crystalemulsified water droplet coaggregates increased significantly from 18.35% to 31.98%, and the marginal distance increased from 16.37 μm to 17.36 μm . This showed that with the aggregation of water droplets, wax crystals approached the water droplets, and the area of the formed coaggregates increased. Because the aggregation of microscopic units led to their uneven distribution, the distance increased between the coaggregates.

Therefore, in stage II, the aggregation of emulsified water droplets was the most significant, and it played a decisive role in the further evolution of the microstructure of the system. In previous studies, many scholars mentioned the phenomenon of droplet aggregation or flocculation (Schramm, 1992), but there was little microscopic evidence. This paper provides direct microscopic

images to show the aggregation behaviour of emulsified water droplets. Fig. 11 was some of the motion sequence images captured from the microscopic video, which can be further used to analyse the dynamic aggregation behaviour of emulsified water droplets.

Fig. 11 shows that the aggregation of emulsified water droplets resulted from van der Waals forces between water droplets, which had a significant impact on relatively close water droplets (Fig. 11(b)). Because the smaller water droplets had larger specific surface areas, the effect of van der Waals forces was more significant, and the aggregation of water droplets was promoted. The main factor causing their aggregation with distant water droplets was thermal convection (Fig. 11(a)). In this set of images, when the field of view was fixed, the positions of the emulsified water droplets changed significantly, indicating that they had significant movement behaviours. Since this stage of the experiment was a cooling process, as the temperature decreased, there was a slight temperature difference in the emulsion system that generated thermal convection to drive the water droplets to move, and the moving water droplets adsorbed and form aggregates. Due to the different sizes of water droplets, their inertias were different, and their movement speeds and intensities under convection differed. In addition, a certain microflow developed inside the system due to the temperature drop. These microscale flows moved not only water droplets but also wax crystals. Because of the smaller size of the wax crystals, their motion was more violent, and they collided more easily with water droplets, adsorbed on the surfaces of water droplets, or filled gaps between adjacent water droplets, which led to the formation of the wax crystal-emulsified water droplet coaggregates. Therefore, although the microflow in the waxy crude oil emulsion occurred only on the microscale, it had a direct impact on the microbehaviour of the emulsified water droplets and wax crystals and determined the formation and development of aggregated structures, which in turn affected the evolution of the



(c) Dynamic aggregation of emulsified water droplets under the combined action of van der Waals forces and thermal convection

Fig. 11. Image of the dynamic aggregation process of emulsified water droplets.

gel structure of waxy crude oil emulsions. According to the above analysis, we speculated that when there were more small-sized water droplets and small-sized wax crystals in the waxy crude oil emulsion, the aggregation in the system was more significant, and the aggregation structure was more complex. This may be part of the reason for the different macroscopic rheology properties corresponding to different water droplet and wax crystal size distributions.

Stage III: Temperature 28 °C-20 °C. As shown in Fig. 8, aggregation between emulsified water droplets continued to occur at this stage, and the aggregation tendency was further enhanced with decreasing temperature. Due to the previous aggregation stage, the water droplets were brought close to and in contact with each other. The aggregation at this stage made the water droplets further overlap and accumulate to form a certain spatial structure. Intuitively, compared with the previous stage, the water droplet aggregates shrank, their coverage decreased, and the threedimensional structure was more pronounced. This change resulted in an increase in the distance between the different aggregates and an increase in the area within the field of view that was free of water droplets. The tendency of wax crystals to aggregate to water droplets was also enhanced, and some wax crystals were embedded in the voids between adjacent water droplets, which enhanced the structural strength and stability of the aggregates. Some of the wax crystals surrounded the water droplets and continued to grow as the temperature decreased so that the area of the coaggregates continued to increase as the temperature dropped.

From the quantitative data in Fig. 9(a), wax crystals continued to precipitate at this stage, and their area fraction in the visual field increased from 4.44% to 7.34%. The precipitation rate increased slightly compared with the previous stage. The surface area of emulsified water droplets was reduced due to aggregation, but the precipitation rate of wax crystals was not affected. Therefore, to a certain extent, this showed that the precipitation of wax crystals was not directly related to the area, number, and presence of emulsified water droplets. Some images at this stage were extracted to show the state of the wax crystals on the surfaces of the water droplets at this time. As shown in Fig. 12.

Fig. 12 shows that although wax crystals gathered on the surface of the water droplets, their distribution was not uniform, and they did not entirely cover the water droplets. Combined with the above microscopic images, it can be seen that the main reasons for the aggregation of wax crystals on the surfaces of water droplets were microscale flow in the system and van der Waals forces between wax crystals and water droplets. In addition, according to the data in Fig. 9(a), the marginal distance of wax crystals at this stage continued to decrease as the temperature dropped, from 5.89 μm to 5.06 μm . The aggregation of wax crystals was more pronounced, and their interactions were also enhanced.

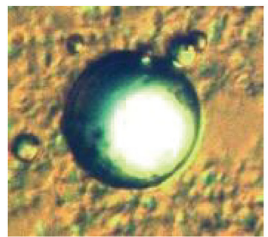
In Fig. 9(b), at this stage, the area fraction of emulsified water droplets decreased with decreasing temperature, from 30.20% to 29.27%. This was related to the large aggregation of water droplets

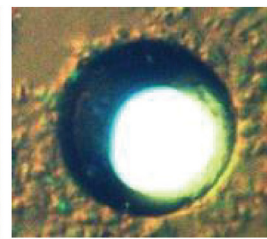
at this stage, which caused them to overlap and accumulate, reducing the coverage of water droplets on the plane. The marginal distance of the water droplets showed a trend of first decreasing and then increasing significantly, from 6.93 µm to 5.42 µm, and then increasing to 14.04 µm. The reason for this was also related to the aggregation of water droplets. Although the aggregation of water droplets reduced the marginal distance, at this stage, the water droplets gradually completed the contact aggregation, and the main aggregation was to promote the mutual overlapping and stacking of the water droplets. As a result, when the algorithm was used to identify the water droplets, the gathered multiple water droplets were regarded as a large water droplet. Then, the marginal distance of the water droplet aggregates was added to the calculation of the water droplet marginal distance in the field of view. Due to the aggregation of water droplets, the distance between adjacent aggregates increased, which led to the situation in which the calculated marginal distance of water droplets increased significantly with decreasing temperature. This change in marginal distance was significant and could signify a substantial shift in droplet aggregation behaviour from close contact to overlapping stacking.

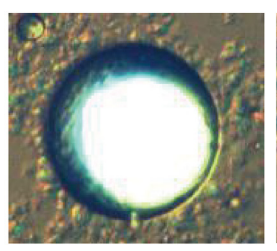
In Fig. 9(c), the area fraction of wax crystal-emulsified water droplet coaggregates first stabilized and then increased slightly. At this stage, although the area of water droplets was reduced due to overlapping and stacking, the effect of the continuous growth of wax crystals on the outside of the water droplets gradually exceeded the effect of the reduction in the area of water droplets. Finally, the area fraction of coaggregates increased slightly with decreasing temperature from 31.98% to 32.81%. At the same time, the marginal distance of the coaggregates first decreased and then increased with decreasing temperature. This trend was also related to the continuous growth of wax crystals on the outside of the coaggregates, which led to an increase in their area. Once different coaggregates came into contact, they were identified as one coaggregate, which led to a trend of decreasing first and then increasing the marginal distance of the coaggregates with decreasing temperature.

Therefore, in stage III, the aggregation phenomenon of wax crystals and emulsified water droplets was significant, and their coaggregates had various complex morphological and three-dimensional structural characteristics. As the temperature decreased, the wax crystals gradually covered the outside of the coaggregates and continued to grow. While increasing the coverage and structural strength of the coaggregates, it also began to inhibit the aggregation and filling of wax crystals and water droplets into the aggregates, thereby making the internal structure and morphology of the coaggregates increasingly stable. To refine the structural characteristics of the wax crystal-emulsified water droplet coaggregates, some representative microscopic images were selected as Fig. 13.

As shown in Fig. 13, in stage III, the coaggregate structure of water droplets and wax crystals had obvious three-dimensional characteristics. The aggregated water droplets were the core







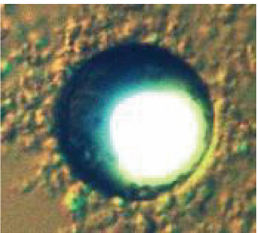
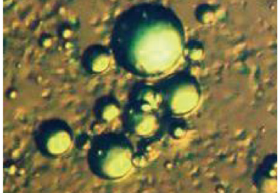
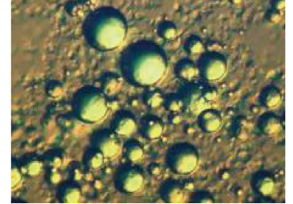


Fig. 12. Presence of wax crystals on the surface of emulsified water droplets.







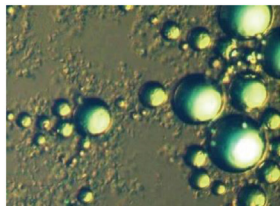


Fig. 13. Micromorphology of wax crystal-emulsified water droplet coaggregates at stage III.

structure. The wax crystals and water droplets stacked and overlapped significantly, which greatly enhanced the structural strength of the coaggregates and made them more stable. Many wax crystals also surrounded the exterior of the coaggregates. As the temperature decreased, these wax crystals continued to grow and increased the areas of the coaggregate. In addition, the initially discrete wax crystals migrated to the outside of the coaggregates to expand their coverage. The wax crystals surrounding the exteriors of the coaggregates made the overall structure and morphology of the coaggregates more stable. Additionally, they inhibited the migration of water droplets and wax crystals into the aggregates.

Stage IV: Temperature 20 °C—16 °C. As shown in Fig. 8, the typical feature of this stage was that the internal morphology and structure of the wax crystal-emulsified water droplet coaggregates were basically stable, but their structure was strengthened due to the growth of interior wax crystals. The density of the internal structure increased. The area of the coaggregates continued to increase due to the continuous growth of the exterior wax crystals and the addition of surrounding wax crystals. The coverage gradually increased, which eventually led to the interconnection of different coaggregates to form a floc structure with more extensive coverage and finally completed the shaping of the waxy crude oil emulsion gel microstructure system.

Fig. 9(a) shows that the number of wax crystals precipitated at this stage continued to increase, but the growth rate slowed, and the wax crystal marginal distance was relatively stable. The emulsified water droplets were at the cores of the coaggregates or flocs. Their area fraction and marginal distance were very stable, indicating that the internal structure and morphology of the wax crystal-emulsified water droplet coaggregates basically did not change with decreasing temperature. The area fraction further increased with the decline in temperature from 32.81% to 35.80%, and its marginal distance further decreased from 16.08 μ m to 13.50 μ m. This showed that as the temperature decreased, the wax crystals around the coaggregates continued to grow at this stage, resulting in an increase in their area and a reduction in the marginal distance between adjacent coaggregates. The time series images visually demonstrate this phenomenon (see Fig. 14).

The areas framed by the different coloured lines in Fig. 14 represent the areas where the coaggregates were separated, that is, occupied by liquid hydrocarbons. It can be seen from the figure that as the temperature decreased, these areas gradually decreased; at the same time, the coverage of the coaggregates

gradually increased, but its internal structure was very stable, which was caused by the continuous growth of wax crystals around the coaggregates.

Therefore, in stage IV, the internal structure characteristic of the W/O waxy crude oil emulsion evolved. The internal structure of the wax crystal-emulsified water droplet coaggregates continued to strengthen. The overall structure was stable, and the coverage increased. Different coaggregates gradually connected to form a larger floc structure, which promoted the system to complete the gelation process.

Based on the experimental analysis results obtained from the experimental oil samples, water samples, and emulsion preparation conditions in this research, the complete description of the microstructure evolution of the W/O waxy crude oil emulsion during the cooling and gelation processes were described as Fig. 15.

Fig. 15 shows that the cooling and gelation process of a waxy crude oil emulsion can be divided into four stages:

Stage I (40 $^{\circ}$ C-36 $^{\circ}$ C): Wax crystals and emulsified water droplets were mainly unaggregated, dispersed and independent. There were small numbers of wax crystal aggregates and wax crystals attached to the surfaces of water droplets to form coaggregates. It was also found that the microscale movement of wax crystals and water droplets make the contribution to the formation of coaggregates.

Stage II (36 °C-28 °C): Emulsified water droplets aggregated, and water droplet aggregates gradually replaced unaggregated water droplets inside the system. The number of wax crystals increased. The wax crystals were prone to aggregation and tended to aggregate with water droplets to form coaggregates. Stage III (28 $^{\circ}\text{C}{-}20$ $^{\circ}\text{C}):$ The aggregation of emulsified water droplets continued, the aggregation tendency strengthened with decreasing in temperature, and the water droplets overlapped and accumulated, forming a certain spatial structure. Compared with stage II, the water droplet aggregates shrank in size, and the three-dimensional structure was more pronounced. Additionally, the tendency of wax crystals to aggregate with water droplets further strengthened, and some wax crystals embedded in gaps between adjacent water droplets to enhance the structural strength of the aggregates. Some wax crystals surrounded the outside of the water droplets and continued to grow as the temperature decreased.

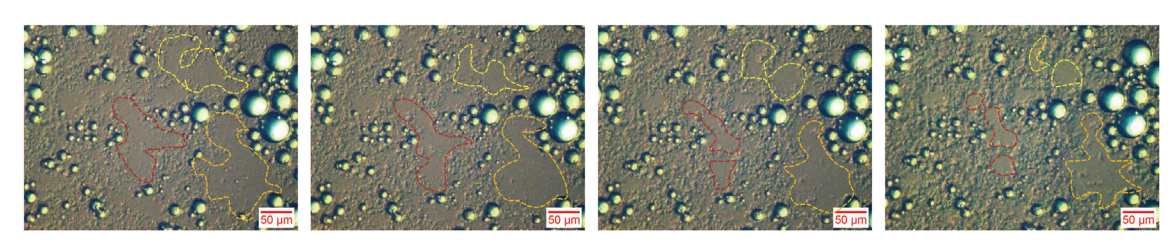


Fig. 14. Continuous growth process of wax crystal-emulsified water droplet coaggregates at stage IV.

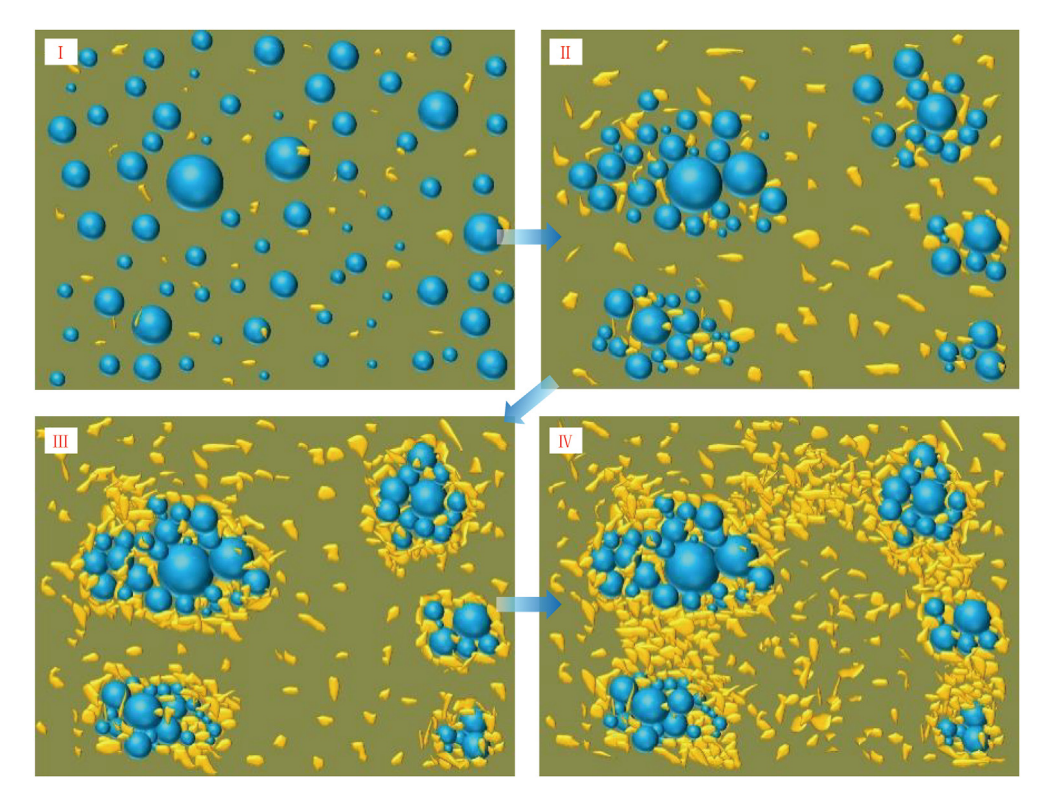


Fig. 15. Schematic diagram of microstructure evolution during cooling and gelation of waxy crude oil emulsions.

Stage IV (20 °C–16 °C): At this stage, the internal morphology and structure of the wax crystal-emulsified water droplet coaggregates were basically stable, and the growth of wax crystals enhanced the coaggregate structure. Additionally, the areas of the coaggregates continued to increase due to the continuous growth of the exterior wax crystals and the addition of the surrounding wax crystals, resulting in the interconnection of different coaggregates to form a larger floc structure, which finally finished the gelation of the waxy crude oil emulsion system.

4.2.3. Correlation between viscoelasticity and microstructure evolution of waxy crude oil emulsions

The macroscopic rheological data show trends corresponding to the evolution of the microstructure of the W/O waxy crude oil emulsions. The rheo-optic in situ synchronous measurement results in Fig. 7 show that in stage I (40 °C-36 °C), the measured viscoelasticity data did not change much, and the synchronous microscopic observation results also showed that the microstructure of the system did not change significantly, the number of precipitated wax crystals was small, and the wax crystals and water droplets were relatively dispersed. In stage II (36 °C-28 °C), the viscoelastic parameters of the system began to increase significantly with increasing precipitation of wax crystals and aggregation tendency of water droplets. In stage III (28 °C-20 °C) not only the precipitation of wax crystals continued to increase, but a large number of coaggregate structures formed between wax crystals and emulsified water droplets, their structural strength increased significantly with decreasing temperature, and the coverage gradually increased, resulting in a significantly faster rise in the viscoelasticity data of the system. In stage IV (20 °C-16 °C), with the continuous precipitation and growth of wax crystals, the coaggregate structure of wax crystals and emulsified water droplets was further enhanced, and the coverage further enlarged. However, in this stage, the wax crystals essentially affected the structural strength of the system, which did not change the growth rate of the viscoelastic data of the system. Therefore, the viscoelasticity of the waxy crude oil emulsions was directly related to the evolution of their microstructure. The evolution process of its microstructure determined the mechanism of the initiation and development of the gelling structure behaviour during the static cooling process.

4.3. Influence and mechanism of water content on gelation behaviour of waxy crude oil emulsions

4.3.1. Rheo-optic in situ synchronisation experimental results

In this section, based on the established experimental techniques and analytical methods, we conducted a comparative study on the viscoelastic parameters and microstructures of emulsion systems with different water contents. We explored the effect of water content on the behaviour and microscopic mechanism of gelation of W/O waxy crude oil emulsions.

Fig. 16 shows that the viscoelastic parameters and microstructures of waxy crude oil emulsions had similar trends with decreasing temperature for different water contents. As the temperature decreased, the viscoelastic parameters of the emulsion system increased, and in different temperature ranges, there were different rates of change. The precipitation of wax crystals, the aggregation of emulsified water droplets, the formation of the coaggregate structure, and the evolution of flocculation structure were all apparent in the experimental results for different water contents. However, there are also significant differences in the experimental results under different water contents. Fig. 17 shows images of the microstructure evolution of the waxy crude oil emulsion with decreasing temperature under different water contents, and we analysed the specific ways that water content affected the microstructure of the emulsion.

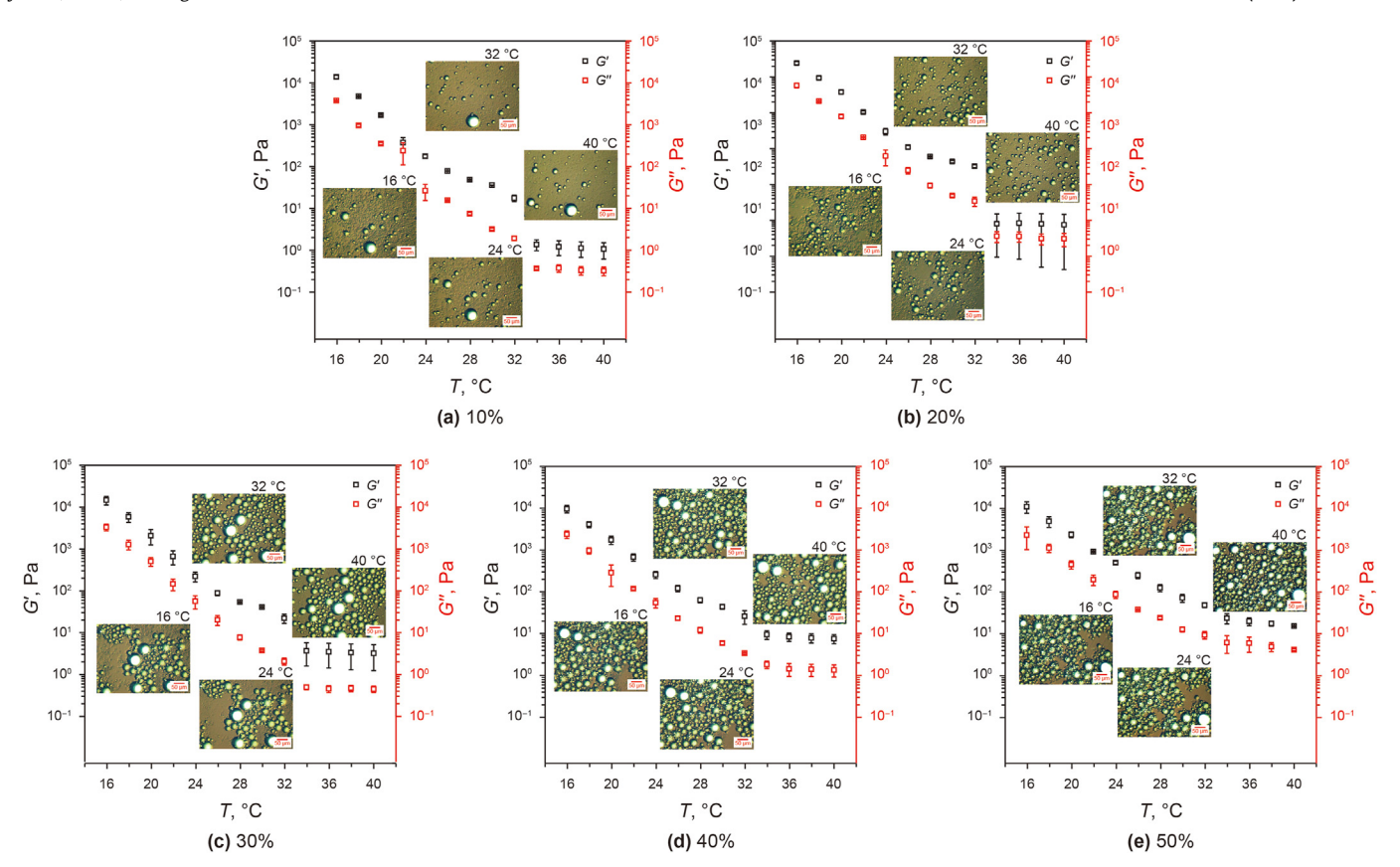


Fig. 16. Variation in viscoelastic parameters and microstructure of W/O waxy crude oil emulsions with temperature for different water contents.

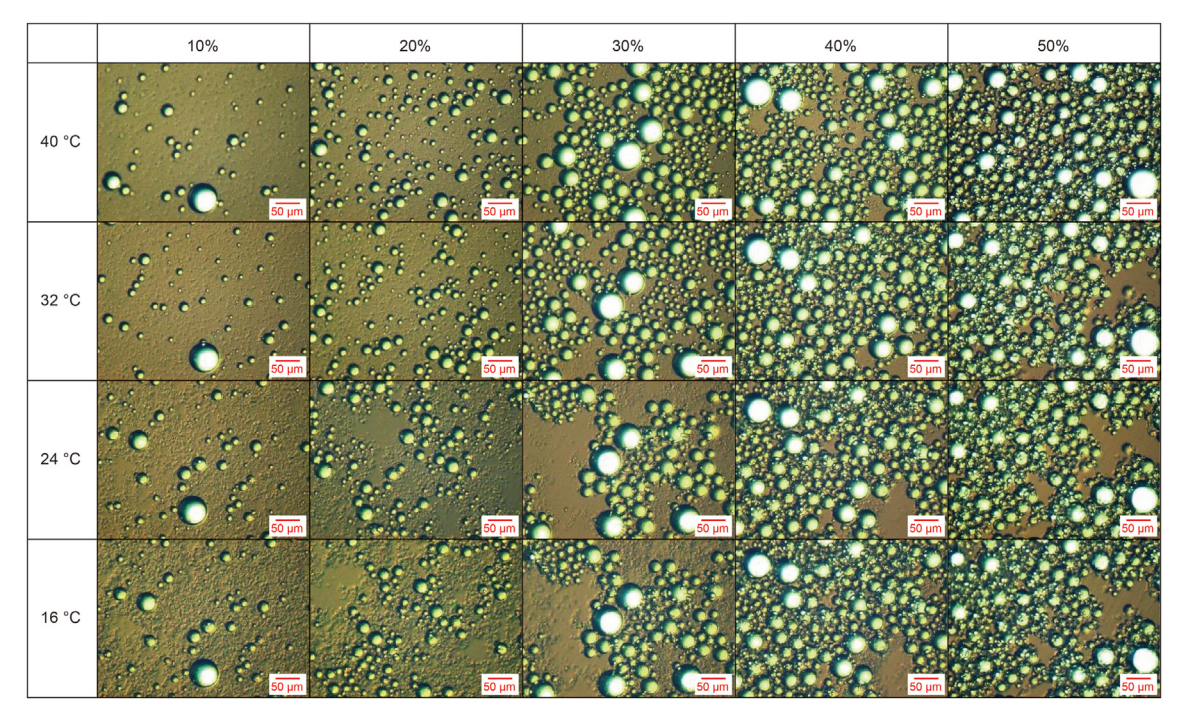


Fig. 17. Microscopic images of emulsion cooling and gelation for different water contents.

With the increase in the number of emulsified water droplets, the number of wax crystals decreased, the aggregation tendency between water droplets became more significant, and a spatial

stacking structure formed. At a lower water content (10%), when the temperature decreased to 16 $^{\circ}$ C, the flocculation structure formed by wax crystals was clearly visible in the microscopic

image. The emulsified water droplets were embedded in the flocculation structure. The mutual connection and aggregation of wax crystals were very significant, and they served as the main skeleton of the flocculation structure. However, with increasing water content, the aggregation of emulsified water droplets became more significant and gradually occupied the main position of the final flocculation structure. The wax crystals were embedded in water droplet aggregates or surrounded by aggregates, which led to the interruption of connections between wax crystals. When the water content was increased to 30%, discontinuous regions of the wax crystal aggregated structure were visible in the microscopic results obtained at 16 °C. With the further increase in water content to 40% and 50%, the area fraction occupied by water droplets was more significant, and the coverage by wax crystals was smaller. This microstructure change will significantly impact the behaviour of the gelling structure of the system. When the water content is low, the network structure formed between wax crystals promotes the gelation of the system. In contrast, at high water content, the flocculation structure formed between the droplets dominates the gelation process of the system (Sun and Zhang, 2016). This is consistent with the microscopic observations in this paper.

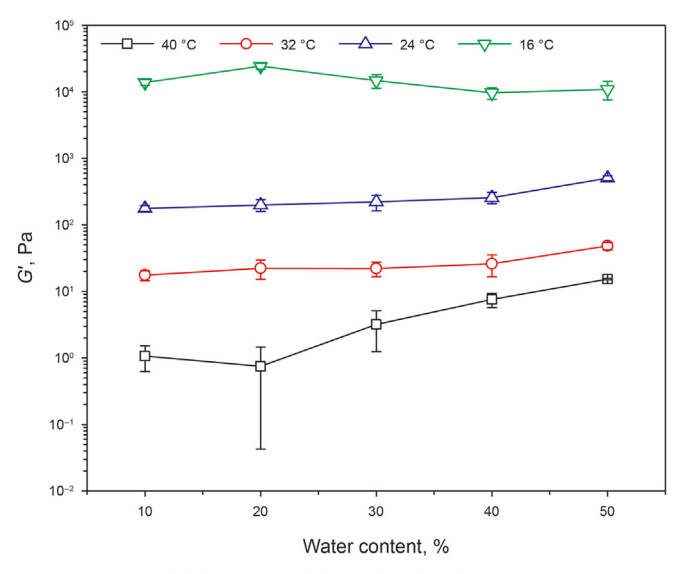
4.3.2. Microscopic mechanism of water content influencing the viscoelasticity of emulsions

Fig. 18 shows the variation in viscoelastic data, such as the storage and loss moduli of waxy crude oil emulsions with water content at different temperatures.

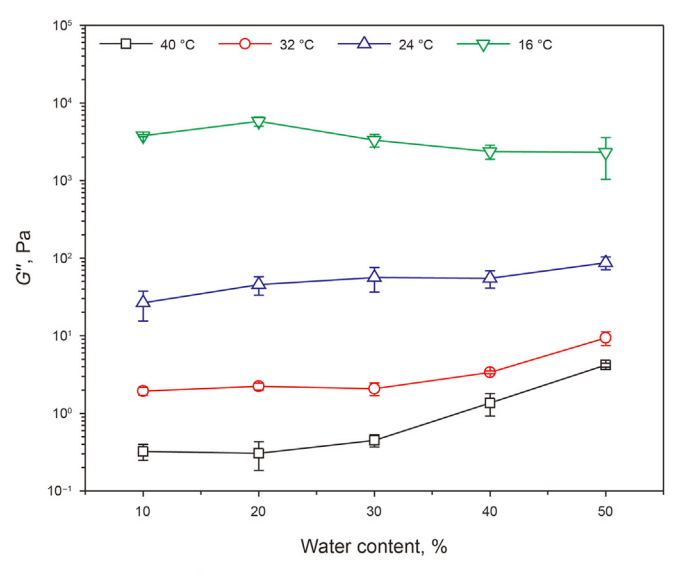
Fig. 18 shows that at different temperatures, the influence of water content on the viscoelastic parameters of the emulsion was distinct. When the temperature was 40 °C, with increasing water content, the viscoelasticity of the emulsion system was significantly enhanced, especially when the water content exceeded 20%, this trend was more obvious. With decreasing temperature, although the viscoelasticity data still showed a trend of increasing with increasing water content, the difference in different water contents gradually decreased. When the temperature decreased to 16 °C, with the rise in water content, the viscoelasticity of the emulsion gel system increased first and then decreased with the increase in water content and reached the maximum value at 20% water content. The influence of water content on the viscoelasticity of

emulsions followed a very complex trend as observed in the studies of other scholars. Some scholars found that with increasing water content, the viscoelasticity of an emulsion system increased (Visintin et al., 2008; Huang and Wang, 2013; Sun et al., 2014; Guo et al., 2016, 2021; Zhang et al., 2019). However, some scholars found that with increasing water content, the viscoelasticity of the system weakened (Peng et al., 2009; Oh and Deo, 2011), Some scholars claimed that a waxy crude oil emulsion had a specific water content corresponding to the maximum viscoelasticity (Paso et al., 2009; Dickinson, 2012). According to the experimental results in Fig. 18, the specific effect of water content on the viscoelasticity of the system was related to temperature and the range of water content. Fig. 19 shows the change in viscoelasticity data of emulsions for different water contents during temperature reduction from 40 °C to 16 °C. When the water content exceeded 20%, the lower the water content of the emulsion was, the more significant the increase in its viscoelastic parameters with decreasing temperature. However, the variation in viscoelastic parameters of the 20% water content emulsion were maximum and exceeded those in the case of 10% water content. Therefore, the various growth rates of the viscoelasticity of emulsions with different water contents with decreasing temperatures were the direct reasons for the effects of water contents on the viscoelasticity of emulsions at several temperatures. Furthermore, the microscopic images in Fig. 17 show that the change rates of the viscoelasticity of the emulsions with varying contents of water with decreasing temperature differed, which was related to the differences in their microstructures. To further illustrate this point, the microscopic images of varying observation fields for various water contents after cooling to 16 °C were extracted to emphasize the essential differences in their internal microstructure for different water contents. As shown in Fig. 20.

In Fig. 20, there were significant differences in the microstructure for different water contents. In addition to the apparent difference in the number of wax crystals and emulsified water droplets, the more significant differences were the connection states between wax crystals, whether a flocculation structure formed between wax crystals, the coverage of the flocculation structure, and the degree of aggregation of water droplets. Combined with the analysis in 4.2, Fig. 20 shows that both wax crystals and emulsified water droplets had a significant impact on the



(a) Storage moduli as a function of water content



(b) Loss moduli as a function of water content

Fig. 18. Variation in viscoelastic parameters of emulsions with water content at different temperatures.

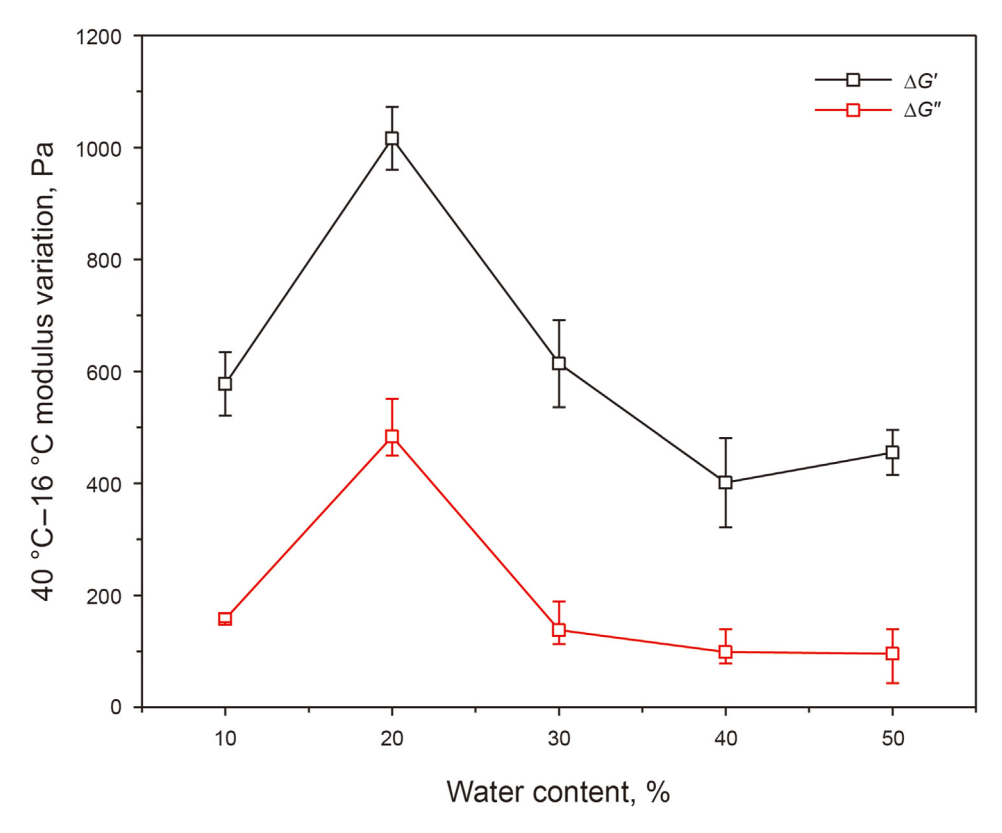


Fig. 19. Variation in the viscoelastic parameters of the emulsion for different water contents.

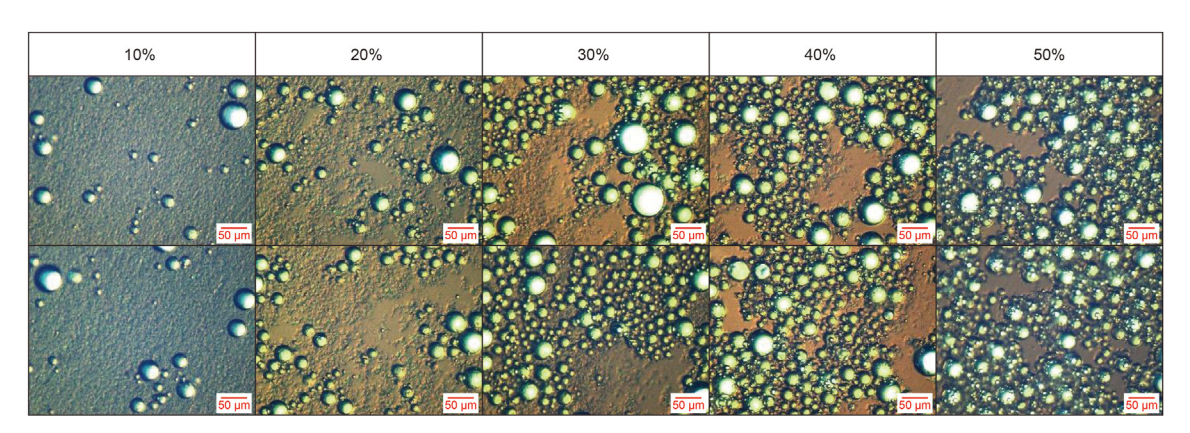


Fig. 20. Microscopic images of emulsions with different water contents after cooling to 16 °C.

viscoelasticity of waxy crude oil emulsion systems. Nevertheless, the influence of wax crystals was more dominant than that of emulsified water droplets. Several microscopic units defined in 4.1 had different degrees of impact on the viscoelasticity of the system. With the differences in water content and temperature, the microstructure formed by wax crystals varied, and the proportion of several microscopic units in the system also differed, which led to the differences in the macroscopic viscoelasticity of the system. The details were as follows:

(1) The flocculation structure formed by wax crystals had the most significant influence on the viscoelasticity of the system. The more complete the flocculation structure formed by the interconnected wax crystals was, the more extensive the coverage, the closer the mutual contact of the wax crystals in the flocculation structure, and the greater the viscoelasticity of the system. This was because when the water content was less than 20% and the temperature was less than 20 °C, the viscoelasticity of the system was significantly enhanced with decreasing temperature. A complete flocculation structure gradually formed between wax crystals. The lower the temperature was, the wider the connection and coverage of the wax crystal flocculation structure, and the stronger the interaction between wax crystals in the structure, which significantly enhanced the viscoelasticity of the system. In contrast, for emulsions with a water content of more than 30%, the presence of many water droplets and their aggregates hindered the formation of wax crystal flocculation structures, which weakened the tendency of the

viscoelasticity of the system to increase with decreasing temperature in this water content range.

- (2) The coaggregates of wax crystals and emulsified water droplets also significantly enhanced the viscoelasticity of the system, but their effect was weaker than that of the wax crystal flocculation structure. With increasing water content, the agglomeration of water droplets was enhanced. Under its influence, wax crystals strengthened the aggregation of water droplets, which were embedded or wrapped on the exterior of the water droplet aggregates to form coaggregates. The addition of wax crystals enhanced the strength of the coaggregates, stronger than the simple aggregation effect of water droplets but weaker than the effect of the wax crystal flocculation structure. Therefore, when the temperature was greater than 20 °C, no large-scale wax crystal flocculation structure formed in the emulsion with a low water content. With increasing water content, the number of coaggregates of wax crystals and emulsified water droplets and the viscoelasticity of the emulsion increased. When the water content was 20% and the temperature dropped to 16 °C, both the wax crystals and the emulsified water droplets coaggregates were present in the emulsion, and a coherent flocculation structure formed between the wax crystals. Hence, the viscoelasticity of the system was the strongest. When the water content was 10%, due to the small number of water droplets, although the wax crystal flocculation structure was present in the system, there were no contributions from the wax crystal-emulsified water droplet coaggregates, so the viscoelasticity of the system was less than 20%. When the water content was in the range from 30% to 50%, due to the large proportion of water droplets, the agglomeration effect was strong, and many wax crystals were attracted, gathered, or embedded in the water droplet aggregates. Although this enhanced the effect of the coaggregates, it consumed many wax crystals, which prevented the formation of flocculated structures between wax crystals, resulting in a case where the strength of the microstructure was weaker than 10% and 20%.
- (3) The aggregates formed between wax crystals enhanced the viscoelasticity of the emulsion system. However, when the number of aggregates was small, their area was small, and a large-scale flocculation structure did not form, and the effect of enhancing the viscoelasticity of the system was not as good as that of the wax crystal flocculation structure and the wax crystal-emulsified water droplet coaggregates.
- (4) The aggregation of the simple emulsified water droplets also enhanced the viscoelasticity of the system, but its effect was weaker. This increased the viscoelasticity of the emulsions with increasing water content in the higher temperature range where wax crystals did not precipitate substantially.
- (5) Although the presence of individual emulsified water droplets enhanced the viscoelasticity of the system, their effect was the weakest.

In summary, the decisive factor for the viscoelasticity of the waxy crude oil emulsion was wax crystals, and the greater their number, the greater the viscoelasticity of the system. However, when the total number of wax crystals was constant, the structures mainly involved in the formation of wax crystals, and the viscoelasticity of the system were different. When the temperature was high and the precipitation of wax crystals was not sufficient to form an overall flocculation structure, the emulsion with a higher water content had more water droplets and more significant aggregation, and it attracted wax crystals to form more coaggregate structures. This made the viscoelasticity of the system increase as the water

content increased. However, when the temperature decreased and the number of wax crystal precipitates increased so that they formed a flocculation structure, the higher the water content of the emulsion was, the stronger the attraction of water droplets to the wax crystals, the more wax crystals were consumed to form coaggregates, and the more hindered the formation of the wax crystal flocculation structure. As a result, with increasing water content, the viscoelasticity of the emulsion decreased. Only when the number of wax crystals and emulsified water droplets reached a certain ratio (for example, the 20% water content in this experiment, when the temperature was less than 20 °C) did wax crystals form coaggregates with emulsified water droplets, and the remaining wax crystals formed an overall flocculation structure. Under these conditions, the viscoelasticity of the emulsion was the highest. This finding was also mentioned in the studies of other scholars (Paso et al., 2009; Dickinson, 2012).

5. Conclusion

In this research, an emulsion prepared with typical waxy crude oil from Hulunbuir Oilfield (the wax content was 16.34%, the resins content was 11.8%, and the asphaltene content was 4.4%) and purified water under the condition of 1000 rpm and water content in the range of 10%—50% were used as the experimental material. The viscoelastic parameters and microstructure evolution of the waxy crude oil emulsion during cooling were systematically investigated by improved rheo-optic in situ synchronous measurement technology. The following outcomes were obtained:

- (1) A rheo-optic in situ synchronous measurement system was modified by improving the light source, building a multiangle composite light source and used for the synchronous observation of wax crystals and emulsified water droplets. Based on this new technique, the macroscopic structural behaviour and microscopic mechanism during gelation of waxy crude oil emulsions was investigated.
- (2) The microstructure of W/O waxy crude oil emulsion had the evolution of "individual structure-homogeneous aggregate structure-heterogeneous coaggregate structure-floc structure" during the static cooling. According to the quantitative data and the microscopic observations, it can be divided into four stages:

Stage I (40 °C-36 °C): Wax crystals and emulsified water droplets were mainly unaggregated, dispersed and independent. There were small numbers of wax crystal aggregates and wax crystals attached to the surfaces of water droplets to form coaggregates. It was also found that the microscale movement of wax crystals and water droplets make the contribution to the formation of coaggregates.

Stage II (36 $^{\circ}$ C–28 $^{\circ}$ C): Emulsified water droplets aggregated, and water droplet aggregates gradually replaced individual water droplets. The number of wax crystals increased. The wax crystals were prone to aggregation and tended to aggregate with water droplets to form coaggregates.

Stage III (28 °C–20 °C): Compared with stage II, the water droplets overlapped and accumulated, the aggregates shrank in size, and the three-dimensional structure was more pronounced. Additionally, the wax crystals gathered further with the water droplets, and some embedded in gaps between adjacent water droplets, some surrounded the outside of the water droplets and continued to grow as the temperature decreased.

Stage IV ($20\,^{\circ}\text{C}-16\,^{\circ}\text{C}$): The growth of wax crystals inside the coaggregates enhanced the coaggregate structure. The areas of the coaggregates continued to increase due to the continuous growth of the exterior wax crystals and the addition of the surrounding wax crystals, resulting in the interconnection of different coaggregates to form a larger floc structure, which finally finished the gelation of the system.

- (3) The viscoelasticity of the waxy crude oil emulsions was directly related to the evolution of their microstructure. In stage I, the viscoelasticity data and the microstructure did not change much. In stage II, the viscoelastic parameters began to increase with increasing precipitation of wax crystals and aggregation tendency of water droplets. In stage III, the precipitation of wax crystals continued to increase, many coaggregate structures formed, resulting in a significantly faster rise in the viscoelasticity data. In stage IV, with the continuous precipitation and growth of wax crystals, the coaggregate structure was further enhanced, and the coverage further enlarged, and gradually evolved to a flocculation structure. However, in this stage, the wax crystals essentially affected the structural strength of the system, which did not change the growth rate of the viscoelastic data of the system.
- (4) At lower water content, the gelling structure of the system was wax crystal flocculation structure as the skeleton, and the emulsified water droplets were embedded in it. With increasing water content, the aggregation of emulsified water droplets occupied the main position. The wax crystals were embedded in water droplet aggregates or surrounded the outside. Only when the number of wax crystals and emulsified water droplets reached a certain ratio, did wax crystals form coaggregates with emulsified water droplets, and the remaining wax crystals formed an overall flocculation structure. Under this condition, the viscoelasticity of the waxy crude oil emulsion was the highest.
- (5) Both wax crystals and emulsified water droplets had an impact on the viscoelasticity of the system. The influence of wax crystals was more dominant than that of emulsified water droplets. The degree of influence of several microscopic units on the viscoelasticity of the system is as follows: the flocculation structure formed by wax crystals > the coaggregates of wax crystals and emulsified water droplets > the aggregates formed between wax crystals > the aggregation of the simple emulsified water droplets > individual emulsified water droplets.

Declaration of competing interest

There is no conflict of interest.

Acknowledgements

This work is supported by the Natural Science Foundation of Heilongjiang Province (LH 2021E018).

References

- Arganda-Carreras, I., Kaynig, V., Rueden, C., Eliceiri, K.W., Schindelin, J., Cardona, A., Sebastian Seung, H., 2017. Trainable Weka Segmentation: a machine learning tool for microscopy pixel classification. Bioinformatics 33 (15), 2424–2426. https://doi.org/10.1093/bioinformatics/btx180.
- Blake, A.I., Marangoni, A.G., 2015. The effect of shear on the microstructure and oil binding capacity of wax crystal networks. Food Biophys. 10 (4), 403–415. https://doi.org/10.1007/s11483-015-9398-z.
- Breiman, L., 2001. Random forests. Mach. Learn. 45 (1), 5–32. https://doi.org/ 10.1023/A:1010933404324.

Del Valle, A., Torra, J., Bondia, P., Tone, C.M., Pedraz, P., Vadillo-Rodriguez, V., Flors, C., 2020. Mechanically induced bacterial death imaged in real time: a simultaneous nanoindentation and fluorescence microscopy study. ACS Appl. Mater. Interfaces 12 (28), 31235—31241. https://doi.org/10.1021/acsami0c08184

- Dickinson, E., 2012. Emulsion gels: the structuring of soft solids with protein-stabilized oil droplets. Food Hydrocolloids 28 (1), 224–241. https://doi.org/10.1016/j.foodhyd.2011.12.017.
- Dong, H., Zhao, J., Wei, L.X., Liu, Y., Li, Y.H., 2020. Effect of initial cooling temperature on structural behaviors of gelled waxy crude oil and microscopic mechanism investigation. Energy Fuels 34 (12), 15782–15801. https://doi.org/10.1021/ acs.energyfuels.0c02274.
- Fan, K.F., Li, S., Li, R.B., 2021. Micro-mechanism analysis of the rheological properties of water-in-waxy-crude-oil emulsion under pipe flow. J. Dispersion Sci. Technol. 43 (1), 114–125. https://doi.org/10.1080/01932691.2020.1823231.
- Feng, C.N., Zhang, D.K., Chen, K., Guo, Y.B., Hao, T.Q., 2017. Research on in-situ microscopic observation of dynamic contact and reciprocating sliding friction of GM-3 lining interface. Tribol. Int. 115, 179–190. https://doi.org/10.1016/ i.triboint.2017.05.023.
- Guo, L.P., Han, X., Lei, Y., Wang, L., Yu, P.F., Shi, S., 2021. Study on the thixotropy and structural recovery characteristics of waxy crude oil emulsion. Petrol. Sci. 18 (4), 1195–1202. https://doi.org/10.1016/j.petsci.2021.07.003.
- Guo, L.P., Shi, S., Wang, Y., 2016. Study on viscoelastic behaviors of waxy crude water-in-oil emulsion. Adv. Chem. Eng. Sci. 6 (2), 209–215. https://doi.org/ 10.4236/aces.2016.62022
- Guo, L.P., Zhang, J.J., Sun, G.Y., Bao, Y.Q., 2015. Thixotropy and its estimation of water-in-waxy crude emulsion gels. J. Petrol. Sci. Eng. 131, 86–95. https:// doi.org/10.1016/j.petrol.2015.04.032.
- Haj-shafiei, S., Ghosh, S., Rousseau, D., 2013. Kinetic stability and rheology of waxstabilized water-in-oil emulsions at different water cuts. J. Colloid Interface Sci. 410, 11–20. https://doi.org/10.1016/j.jcis.2013.06.047.
- Huang, Q.Y., Wang, L., 2013. Effect of droplet distribution on rheological properties of water-in-oil emulsion in waxy crude oils. Acta Pet. Sin. 34 (4), 765. https:// doi.org/10.7623/syxb201304019.
- Jiang, Y.M., Li, C.X., 2000. Preparation of oil-water emulsion. Gasf. Surf. Eng. (6), 21–22. https://doi.org/10.3969/j.issn.1006-6896.2000.06.010 (in Chinese).
- Kane, M., Djabourov, M., Volle, J.L., Lechaire, J.P., Frebourg, G., 2003. Morphology of paraffin crystals in waxy crude oils cooled in quiescent conditions and under flow. Fuel 82 (2), 127–135. https://doi.org/10.1016/S0016-2361(02)00222-3.
- Koumakis, N., Petekidis, G., 2011. Two step yielding in attractive colloids: transition from gels to attractive glasses. Soft Matter 7 (6), 2456–2470. https://doi.org/ 10.1039/COSM00957A.
- Lee, H.M., Lee, J.W., Park, O.O., 1997. Rheology and dynamics of water-in-oil emulsions under steady and dynamic shear flow. J. Colloid Interface Sci. 185 (2), 297–305. https://doi.org/10.1006/jcis.1996.4592.
- Li, S., Huang, Q.Y., Wang, L., Fan, K.F., 2015. Research on viscoelastic properties of water in waxy crude oil emulsion gels with the effect of droplet size and distribution. Can. J. Chem. Eng. 93 (12), 2233–2244. https://doi.org/10.1002/ cjce.22324.
- Li, Y.H., Zhao, J., Dong, H., Xi, X.R., 2021. The role of shearing effect in the evolution of the microscopic behavior of wax crystals. New J. Chem. 45 (23), 10418–10431. https://doi.org/10.1039/D1NJ01407B.
- Lin, N.Y., McCoy, J.H., Cheng, X., Leahy, B., Israelachvili, J.N., Cohen, I., 2014. A multi-axis confocal rheoscope for studying shear flow of structured fluids. Rev. Sci. Instrum. 85 (3), 033905. https://doi.org/10.1063/1.4868688.
- Liu, Y., Zhuge, X.L., Wang, Z.H., Zhang, L., 2019. Waxy crystal morphology and aggregation behavior under the influence of waxy crude oil emulsification mechanism. Oil Gas Storage Transp. 38 (8), 877–884 (in Chinese).
- Ma, Q.L., Wang, W., Wang, C.S., Gong, J., 2019. Experimental investigation of entrapped water droplets in wax deposition from water-in-oil emulsion considering wax crystals adsorption at the oil—water interface. Energy Fuels 34 (2), 1601–1607. https://doi.org/10.1021/acs.energyfuels.9b03804.
- Oh, K., Deo, M.D., 2011. Yield behavior of gelled waxy oil in water-in-oil emulsion at temperatures below ice formation. Fuel 90 (6), 2113–2117. https://doi.org/10.1016/j.fuel.2011.02.030.
- Pal, R., 1996. Effect of droplet size on the rheology of emulsions. AIChE J. 42 (11), 3181–3190. https://doi.org/10.1002/aic.690421119.
- Paso, K., Silset, A., Srøland, G., Gonçalves, M.D.A., Sjoblom, J., 2009. Characterization of the formation, flowability, and resolution of Brazilian crude oil emulsions. Energy Fuels 23 (1), 471–480. https://doi.org/10.1021/ef800585s.
- Peng, J.X., Xia, H.Y., Liu, K.Q., Gao, D., Yang, M.N., Yan, N., Fang, Y., 2009. Water-in-oil gel emulsions from a cholesterol derivative: structure and unusual properties. J. Colloid Interface Sci. 336 (2), 780–785. https://doi.org/10.1016/i.icis.2009.04.055.
- Piroozian, A., Hemmati, M., Safari, M., Rahimi, A., Rahmani, O., Aminpour, S.M., Pour, A.B., 2021. A mechanistic understanding of the water-in-heavy oil emulsion viscosity variation: effect of asphaltene and wax migration. Colloids Surf. A Physicochem. Eng. Asp. 608, 125604. https://doi.org/10.1016/ j.colsurfa.2020.125604.
- Schramm, L.L., 1992. Fundamentals and applications in the petroleum Industry. Adv. Chem. 231, 3–24.
- Shi, B.H., Zhang, Y., Liu, Y., Wang, Q., Song, S.F., Gong, J., 2018. Experimental study and quantitative characterization of microscopic properties of water-in-oil emulsions in flow systems. Oil Gas Storage Transp. 37 (2), 183–189+203. https://doi.org/10.6047/j.issn.1000-8241.2018.02.010 (in Chinese).

- Sun, G.Y., Li, C.X., Yang, F., Yao, B., Xiao, Z.Q., 2017. Experimental investigation on the gelation process and gel structure of water-in-waxy crude oil emulsion. Energy Fuels 31 (1), 271–278. https://doi.org/10.1021/acs.energyfuels.6b02253.
- Sun, G.Y., Zhang, J.J., 2016. Research progress on rheological properties of W/O crude oil emulsion and its gel. Oil Gas Storage Transp. 35 (3), 229–240. https://doi.org/10.6047/j.issn.1000-8241.2018.02.010 (in Chinese).
- Sun, G.Y., Zhang, J.J., Li, H.Y., 2014. Structural behaviors of waxy crude oil emulsion gels. Energy Fuels 28 (6), 3718–3729. https://doi.org/10.1021/ef500534r.
- Teich, E.G., Galloway, K.L., Arratia, P.E., Bassett, D.S., 2021. Crystalline shielding mitigates structural rearrangement and localizes memory in jammed systems under oscillatory shear. Sci. Adv. 7 (20), eabe3392. https://doi.org/10.1126/ sciadv.abe3392.
- Visintin, R.F., Lockhart, T.P., Lapasin, R., D'Antona, P., 2008. Structure of waxy crude oil emulsion gels. J. Non-Newtonian Fluid Mech. 149 (1–3), 34–39. https://doi.org/10.1016/j.jnnfm.2007.07.008.
- Vargas, G.G., Soares, E.J., Thompson, R.L., Sandoval, G.A., Andrade, R.M., Campos, F.B., Teixeira, A., 2018. Emulsion effects on the yield stress of gelled waxy crude oils. Fuel 222, 444–456. https://doi.org/10.1016/j.fuel.2018.01.105.
- Wen, J.B., Zhang, J.J., Wei, M., 2016. Effective viscosity prediction of crude oil-water mixtures with high water fraction. J. Petrol. Sci. Eng. 147, 760–770. https://doi.org/10.1016/j.petrol.2016.09.052.
- doi.org/10.1016/j.petrol.2016.09.052.

 Wong, S.F., Lim, J.S., Dol, S.S., 2015. Crude oil emulsion: a review on formation, classification and stability of water-in-oil emulsions. J. Petrol. Sci. Eng. 135, 498–504. https://doi.org/10.1016/j.petrol.2015.10.006.

- Xia, H.F., Zhang, J.J., 2001. Study on the mechanism of low-speed shear affecting low-temperature fluidity of additive crude oil. Oil Gas Storage Transp. 20 (2), 32–34. https://doi.org/10.3969/j.issn.1000-8241-D.2001.02.008 (in Chinese).
- Yan, D.F., Luo, Z.M., 1987. Rheological properties of Daqing crude oil and their application in pipeline transportation. SPE Prod. Eng. 2 (4), 267–276. https:// doi.org/10.2118/14854-PA.
- Yu, G.M., Zhong, W.X., Zhang, Y.Y., 2021. Review and prospect of global oil and gas exploration and development in 2020. World Petroleum Industry 28 (2), 9-17+24 (in Chinese).
- Zhang, Y.X., Li, S., Wang, W.Q., Wang, G.F., Xiang, N., Huang, Y., 2019. Analysis of water content on rheology and wax precipitation characteristics. J. Petrochem. Univ. 32 (2), 71. https://doi.org/10.3969/j.issn.1006-396X.2019.02.012 (in Chinese)
- Zhang, Y., Gong, J., Ren, Y.F., Wang, P.Y., 2010. Effect of emulsion characteristics on wax deposition from water-in-waxy crude oil emulsions under static cooling conditions. Energy Fuels 24 (2), 1146–1155. https://doi.org/10.1021/ef901065c.
- Zhao, J., Xi, X.R., Dong, H., Li, Y.H., Jiang, M.Z., 2021. In situ observation of microscopic motions and the structure dynamic transformation of wax crystals in waxy crude oil subjected to shear. New J. Chem. 45 (37), 17522–17543. https://doi.org/10.1039/D1N|02292|.
- Zhao, J., Zhao, W.Q., Dong, H., Wei, L.X., Liu, Y., 2020. New approach for the in situ microscopic observation of wax crystals in waxy crude oil during quiescent and dynamic cooling. ACS Omega 5 (20), 11491–11506. https://doi.org/10.1021/acsomega.0c00606.